IMAGE CLASSIFICATION AND INITIAL ORBIT DETERMINATION OF RESIDENT SPACE OBJECTS (RSO)

ANDREA VALLECILLO BAIRES

A THESIS SUBMITTED TO

THE FACULTY OF GRADUATE STUDIES

IN PARTIAL FULFILLMENT OF THE REQUIREMENTS

FOR THE DEGREE OF MASTER OF SCIENCE

GRADUATE PROGRAM IN EARTH AND SPACE SCIENCE

YORK UNIVERSITY

TORONTO, ONTARIO

JANUARY 2024

Abstract

The importance of Space Situational Awareness (SSA) research is steadily growing due to continuous launches of new technologies, leading to increased congestion and potential collisions in Earth's orbit. Optical imagers, based in both ground and space, serve as important tools for observing, detecting, and studying resident space objects (RSOs). Optical imagers capture vast amounts of data that can be used for different applications in SSA research. However, manually inspecting and classifying these images for specific purposes is a time-consuming task. Implementing an automated image classification can streamline the labelling process for optical databases to expedite SSA research. Another significant aspect of SSA research and RSO tracking using optical images involves reliable object identification and Orbit Determination (OD). Angles-only Initial Orbit Determination (IOD) methods are often employed as a starting point to optimize the OD process. These advancements play a pivotal role in enhancing and contributing to SSA research.

Acknowledgements

I am deeply grateful for the all the support I have received throughout my graduate studies. To my peers, thank you for your invaluable encouragement and collaborative spirit. Special thanks to my mentors among them, whose wisdom and guidance steered my growth. A special mention goes to my professor, Dr. Regina Lee, whose support, and constructive challenges have pushed me, fostering continual growth and improvement. Her mentorship has been transformative, inspiring me to strive for excellence in every endeavor. I'm deeply appreciative of my partner, whose unwavering support and encouragement has been a constant source of motivation and strength. Finally, I would like to thank my parents, whose unwavering love and support have been the foundation of my journey. To my mother, whose countless sacrifices have paved the way for opportunities. To my father, whose nurturing of my curiosity and unwavering belief in my abilities from a young age have been the catalyst for my pursuit of knowledge. His constant encouragement to reach for the stars has instilled in me the resilience to strive for my aspirations.

Table of Contents

List of Tables

List of Figures

List of Acronyms

Acronym	Definition
RSO	Resident Space Object
LEO	Low-Earth Orbit
GEO	Geosynchronous Earth Orbit
SSA	Space Situational Awareness
TLE	Two-Line Element
IOD	Initial Orbit Determination
OD	Orbit Determination
LOS	Line-of-Sight
PSF	Point-Spread Function
ASAT	Anti-Satellite
CSA	Canadian Space Agency
FOV	Field of View
RSONAR	Resident Space Object Near-space Astrometric Research
NEOSSat	Near-Earth Object Surveillance Satellite
DRDC	Defence Research and Development Canada
HEOSS	High Earth Orbit Space Surveillance
TRM	Track Rate Mode
FAI	Fast Auroral Imager
CASSIOPE	Cascade SmallSat and Ionospheric Polar Explorer
CCD	Charged-Couple Device
SBOIS	Space-Based Optical Image Simulator

Chapter 1: Introduction

1.1: Motivation

Earth's resident space objects (RSOs) are objects which reside in the planet's orbit and include objects such as satellites, natural objects, and space debris [1]. There are about 23,000 trackable objects in Low-Earth (LEO) and Geosynchronous Earth (GEO) orbits of which about 4,800 are satellites [1]. RSOs play significant and critical roles in various aspects of society and scientific research. For instance, satellites are utilized in everyday tasks such as navigation, electronic transactions, and live sports broadcasting [2]. Moreover, they contribute extensively to fields like health and climate research, as well as supporting the agriculture industry with weather information [2]. The invaluable applications and diverse roles fulfilled by RSOs emphasize their crucial value as assets in society, demanding their utmost protection.

Space Situational Awareness (SSA) is a rapidly evolving field which is critical for space operations and safety, as it provides the necessary information to detect and predict the location and trajectory of objects in space, such as satellites, debris, and asteroids [1]. Tracking RSOs allows for the prevention of future collisions by planning and executing prevention maneuvers when needed [1]. As the number of both active and inactive satellites, debris, and other objects continue to rise, SSA is becoming a more important and crucial field of research. The growing number of Resident Space Objects (RSOs) leads to a rapid increase in orbital congestion and the likelihood of unwanted collisions. This creates clouds of space debris that can cause further damage to space assets and are more difficult to detect due to their small size. Since space is so vast, it could be believed that there should be sufficient room in orbits for all space technology. However, due to the nature of the current technology and their applications there is a specific

region and distance from Earth which is ideal for all the RSOs. For this reason, those ideal regions are becoming overcrowded. This congestion is evident in Figure 1.1, illustrating the crowding of RSOs in Earth's orbits [1][3].

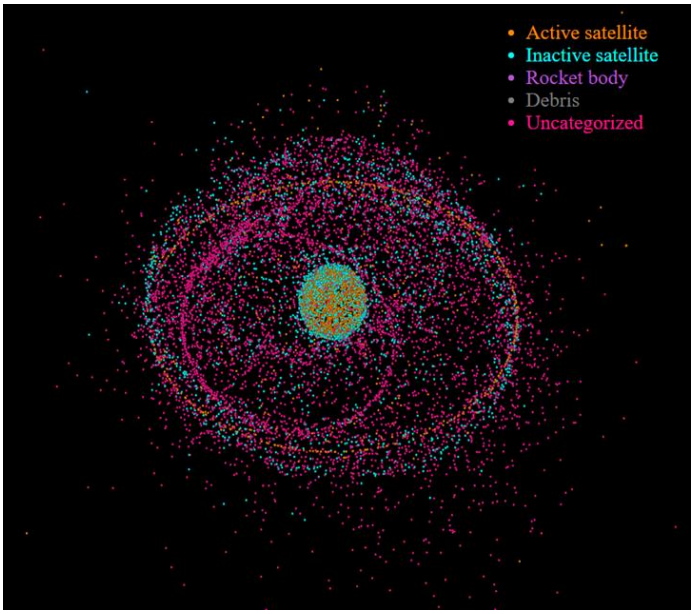

Figure 1.1: Generated image illustrating Earth's RSO population (objects not to scale)

Furthermore, gaining a complete understanding of how RSOs are spread out at different altitudes is crucial for getting a clear picture of the overcrowding situation in our orbits. Figure 1.2 portrays a graph depicting the spatial density of RSOs across different altitudes. This graph provides valuable insights into the distribution patterns and density gradients of RSOs as a function of altitude. Notably, the graph reveals a significant concentration of RSOs in Low-Earth Orbits and at altitudes where specific technological applications are deployed. This observation emphasizes the importance of analyzing congestion in targeted orbits/altitudes, as they rapidly become congested due to the specific purposes and operational requirements of RSOs. It is worth noting that areas with higher density also indicate higher collision risks, highlighting the need for effective strategies to manage orbital congestion [4].

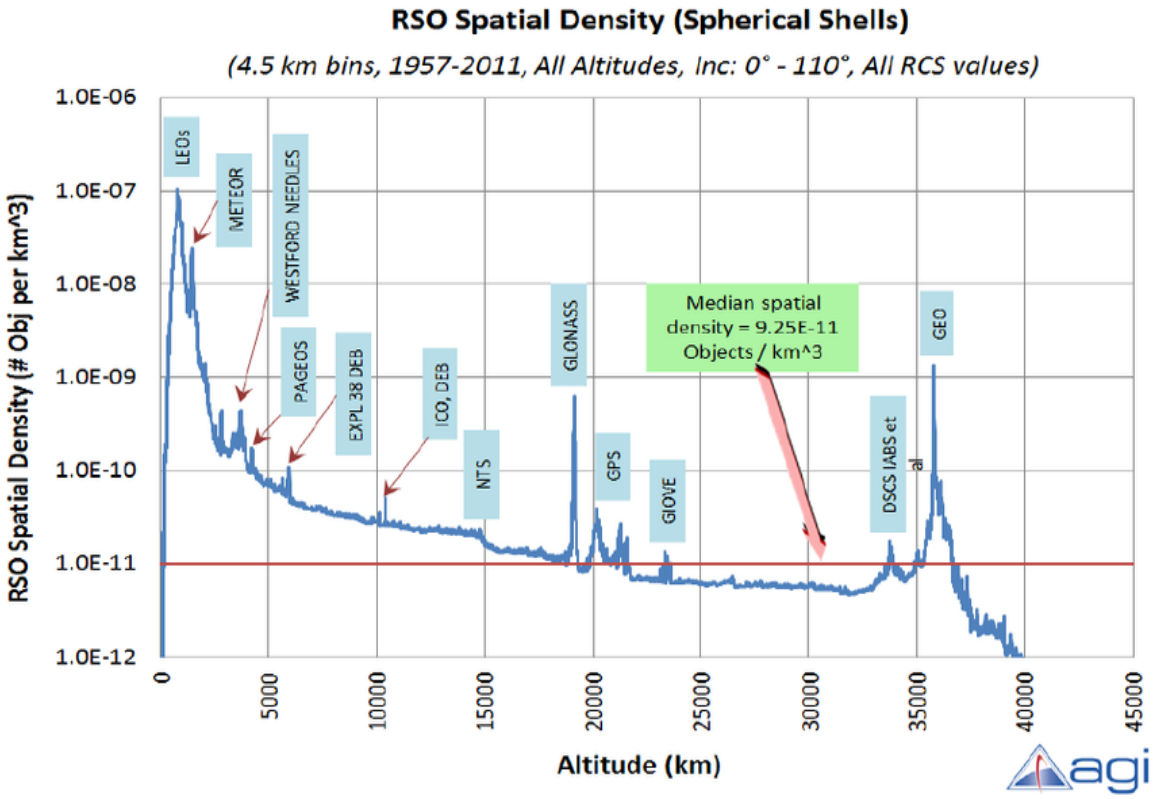

Figure 1.2: RSO population as a function of density vs altitude [4]

As shown in the image, the high density of RSOs in LEO and other altitude ranges reflects the critical role of SSA research in mitigating collision risks and preserving the long-term sustainability of space activities. SSA involves the detection, tracking, and characterization of objects in space to enable the prediction of their future positions and behaviors [1]. It allows for the early identification of potential collision risks and provides the necessary information for space operators to take mitigating actions. In addition, SSA is essential for maintaining the long-term sustainability of space activities by preventing the accumulation of debris and minimizing the risks of collisions that can lead to further debris generation. Thus, SSA is a fundamental aspect of space operations, and its continued development and enhancement are crucial for the safety, sustainability, and security of space activities.

1.2: Research Objectives

Optical imagers, both on the ground and in space, serve as valuable tools for detecting and identifying RSOs. Optical imagers allow scientists to use existing technologies, such as star trackers, and dedicated optical systems for SSA research. Lower resolution images from more cost-effective solutions can also contribute to RSO imaging. Repurposing existing optical imagers and utilizing less expensive hardware solutions present a cost-effective approach to data collection for SSA. The range of imaging systems extends from sophisticated space-based observers to amateur setups using basic telescopes and cameras on the ground. This diversity in available imaging setups enables a broader spectrum of individuals to collect and study images for SSA research. Optical imagers also offer the advantage of covering large areas of the sky swiftly and allow objects above 5,000km altitude to be detected and tracked [5][6]. These advantages make optical imagers a suitable choice for SSA research, including object detection, light curve analysis, and object identification.

Optical imaging solutions can generate large databases after many nights of observations. Sorting through these large amounts of data manually to determine which images are useful for specific SSA research can be time-consuming. Some research such as attitude determination requires images with only star fields, while others focus on unobstructed images of RSO streaks. To streamline the categorization process, algorithms can be developed to automate data analysis and classification, freeing up resources for the development of new SSA strategies. The algorithm developed aims to categorize images by images containing RSO streaks, images with empty star fields, and images containing obstructions or other issues. By leveraging the power of these algorithms, we can improve the efficiency and effectiveness of our SSA efforts, reducing the risk of collisions and the resulting damage to space assets.

One of the strategies for preventing collisions of RSOs is an effective tracking system that can detect, identify, and track all types of RSOs, including satellites, rocket bodies, and other debris. Reliable object identification is crucial for constructing such a tracking system. By confirming an object's predicted trajectory, we can update its Two-Line Element set (TLE) if it deviates from the predicted orbit, contributing to SSA and enabling and advancing current and future collision prevention efforts. A current RSO identification strategy developed by C-CORE involves propagating TLEs of all catalogued objects into the epoch during which an optical observation is made of an orbiting body. Comparing the observed location of the object in the images to the propagated locations, calculated with orthographic projection, yields three correlations of possible identities. However, the accuracy of these correlations is not always accurate as the locations are compared only at the beginning and end of the sequence, along with the line between the two end points.

To address this limitation and improve the accuracy of the identification algorithm, an initial orbit determination (IOD) method is proposed. When dealing with optical images, it is essential to select an IOD method that employs an angles-only approach, considering the available information from optical observations. However, it is important to note that uncertainties can arise in space-based optical measurements due to instrument limitations and measurement errors. Due to these inaccuracies, the accuracy of the IOD output is affected and requires further refinement. Therefore, in the context of space-based observer applications, initial orbit determination serves as an initial guess in an orbit estimation process. The IOD initial guess it generated through three line-of-sight (LOS) observations of the target RSO and the position information of the observer. The initial orbital information is used in an orbit determination (OD) process through which it is refined using an optimization process such as least squares [7]. By

incorporating an orbit estimation process, additional points of comparison are introduced, utilizing the calculated orbital information to enhance the accuracy of the identification algorithm. Moreover, the utilization of IOD helps improve the convergence speed and success of the optimization process, enabling it to converge to an accurate result more efficiently [7]. This approach introduces more points of comparison for existing RSO identification methods, thus contributing to current and future collision prevention efforts.

The ability to predict the identity of the objects more accurately will help to build more robust SSA systems. Figure 1.3 shows an example of an image processing pipeline for SSA research.

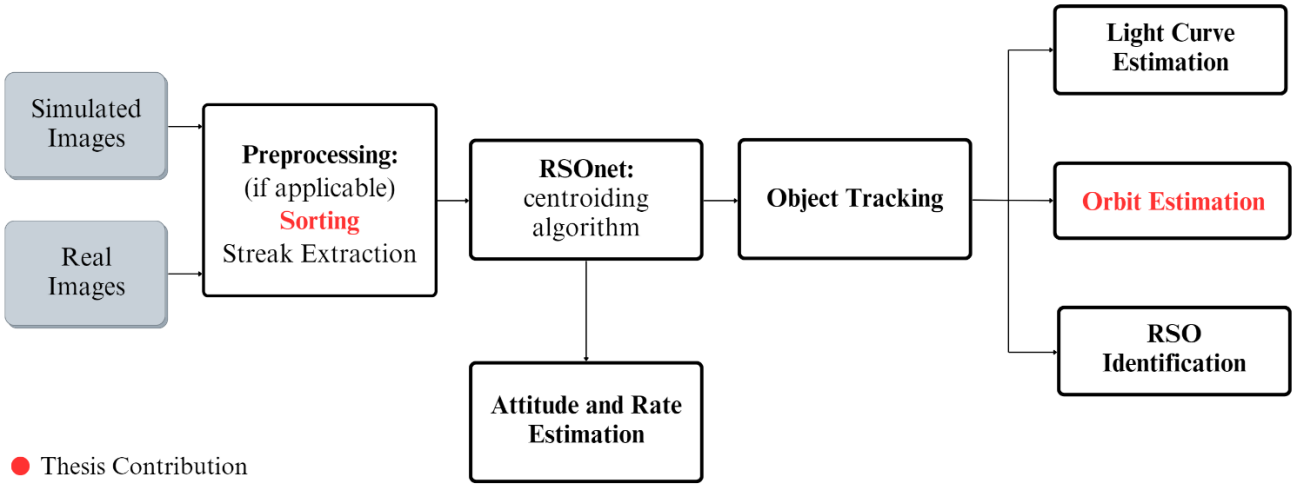

Figure 1.3: Image Processing Pipeline

The image classification research falls under the preprocessing portion as it sorts the images when needed to be used for more specific SSA research. For example, images with just star fields can be fed into the RSOnet program to calculate the centroids of the stars to be used in attitude and rate estimation research. RSOnet is a neural network-based algorithm that was developed by a member of the Nanosatellite Research Lab for accurately determining the

centroids of all objects within images. Meanwhile, images with resident space objects continue through the processing pipeline and object tracking can be done to determine the centroids of a single object in each image the sequence during which the object crossed the camera's field of view. Orbit estimation is done using those centroiding points within the image sequences. There are many techniques for determining the orbital parameters of an object and the results can be used to refine existing orbits or be combined with other information to enhance other research such as RSO identification. Moreover, initial orbit determination is often the first step in the complex process of accurately calculating those parameters. As the field of space technology continues to evolve, the importance of SSA will only grow, making it essential to invest in innovative solutions that can keep pace with the demands of an increasingly congested orbital environment. In summary, this thesis work aims to contribute to SSA research through the following main objectives:

1. Enhance efficiency of SSA research efforts by reducing time spent on manual optical data sorting through the development of an algorithm for automated categorization and analysis of images. This algorithm will specifically identify images with RSO streaks, empty star fields, and those containing obstructions or issues.

2. Strengthen existing RSO identification algorithm by proposing an orbit determination (OD) method which introduces additional points of comparison for the correlation process.

3. Implement an angles-only IOD method for space-based optical measurements. This approach serves as a crucial initial step in the OD pipeline, laying the foundation for subsequent analyses.

1.3: Research Outlook

Chapter 2 will discuss similar technologies in place that aim to improve current SSA effort using similar approaches. It will provide a theoretical background on the techniques employed in this study, including edge detectors and noise filters. In Chapter 3 the focus will be on the image databases that were used in this in this research, along with their respective advantages and limitations. Moving forward, Chapter 4 will discuss the utilization of these databases for the development and testing of an image classification algorithm. This chapter will outline the methodology and results of the detection of RSOs, starfield images, and obstruction detections within each database. Chapter 5 will address the foundational work necessary for improving an existing identification algorithm, with a particular emphasis on implementing Gauss's initial orbit determination. Finally, this dissertation will conclude with a comprehensive discussion of future research and draw conclusions based on the findings presented throughout this study.

Chapter 2: Background

Space Situational Awareness (SSA) research is dedicated to addressing the increasing congestion in Earth's orbits by focusing on ways to protect current and future resident space objects (RSOs). The surge in orbital traffic and reliance on RSOs is creating a high demand for innovative strategies for collision prevention. Consequently, this demand has yielded extensive research exploring diverse methodologies utilizing various data types, including radars and optical images. This research work specifically focuses on SSA approaches employing optical instruments. Optical instruments can reside both on ground and in space, each presenting distinct advantages and limitations. The primary focus lies on image classification and initial orbit determination methods pivotal in advancing SSA endeavors.

2.1: Current Approaches in Space Situational Awareness (SSA) Research

The escalating demand for innovative SSA strategies has given rise to many approaches to deal with congestion in orbital space. This research primarily investigates the use of optical images to aid in mitigation of orbital congestion. Illustrated in Figure 3, the image processing pipeline outlines the spectrum of tasks achievable through optical image analysis within SSA research. This pipeline outlined diverse methods such as image classification, object detection, attitude estimation, and orbit estimation techniques, applicable to both ground-based and space-based observations systems. Current approaches in SSA also involve rapidly evolving methodologies, including integration of machine learning techniques and the adaptation of classical methods to modern practices. The work in this research will touch on an image classification process which utilizes object detection for determining which images contain RSO streaks. Simultaneously, the discussion will extend to initial orbit determination, proposed as the

primary step in enhancing an existing object identification algorithm. These areas of research are integral components of SSA, contributing to the field's advancement.

2.1.1: Optical Image Processing for RSO detection for SSA Research

Optical image databases for SSA research can be substantial, owing to the increased capture of images aimed at mitigating the ongoing problem of space debris. The size of these databases varies depending on factors such as mission length, exposure times, capture frequency, available storage, and downlinking limitations. Whether the data is captured from a ground-based or space-based observer, sifting through the images databases to find useful and relevant data can be a tedious task. While manually sorting and labeling images is an option, it is resource and time consuming and may introduce inaccuracies due to human error. For these reasons, employing image processing techniques to streamline the image sorting process is crucial. There are various existing systems employing image processing techniques address this specific challenge.

Researchers set up a passive ground-based telescope with a fixed line of sight to capture images of the night sky for the goal of RSO detection [8]. An automated process was deployed to process .FITS images captured by the telescope. The image processing pipeline starts with a preprocessing step in which it searches for bright objects, such as stars and satellite streaks, using histograms and appropriate thresholds [8]. An image of just the background information is generated, smoothed, and then subtracted from the original image [8]. Subsequently, the contrast of the resulting image is enhanced before proceeding to the object detection phase [8]. The object detection phase employs techniques such as axis length and connected pixel component analysis and is followed by astrometric calculations of the Right Ascension (RA)/Declination (DEC) of the image [8]. The detected streaks are extracted, their coordinates are correlated in the sky, and

combined to form satellite orbits [8]. This automatic system leverages image processing techniques to reduce the manual labelling workload, expediting SSA research through image analysis.

While this system focused on the detections of satellite streaks, other image processing techniques are used to detect satellites appearing as point sources within images. An example of this is RSOnet, which utilizes machine learning and image processing techniques to classify detected objects within images as stars, RSOs, or different types of noise [9]. This convolutional neural network architecture employed star trackers for the detection, classification, and characterization of multiple objects [9]. RSOnet filters for Point-Spread Function (PSF) shaped objects to find potential stars, RSOs, and noise. It employes three convolutional layers followed by a fully connected layer for the classification of detected objects during tracking [9]. The RSOnet algorithm is particularly useful for images where both the stars and RSOs appear as single point sources. These different methods exemplify how image processing is being used to expedite SSA research on object detection.

2.1.2: Initial Orbit Determination (IOD) for RSOs

IOD plays a critical role in SSA research as it facilitates the study and tracking of RSO orbits. Using optical images and IOD, deviations in predicted RSO orbits can be investigated and TLE information can be updated. Additionally, this process aids with the tracking of RSOs and, potentially, the identification of detected RSOs. IOD methods can vary depending on the kind of information available. There are numerous IOD methods, each with different inputs, processes, accuracies, and limitations. For instance, when range information between the observer and the target RSO is available, different methods are employed compared to instances when optical images do not have range information available. Angles only IOD allows for the determination

of orbital parameters of an observed RSO by using only a minimal number of LOS measurements [10]. These methods are typically used for optical sensors where no range information is available, albeit with some inherent limitations in accuracy [11]. The choice of ideal method depends greatly on specific application requirements and available information.

Table 2.1 provides a summary of some classical angles-only IOD methods and their required information. Note that angular measurements refer to topocentric right ascension and declination [11]. Initial orbit determination encounters many challenges in achieving accurate results. Improving the precision of these calculations is an ongoing focus of SSA research due to its importance in tracking space assets and debris. While some methods focus on using multiple observers to improve accuracy by leveraging different perspectives, other methods prioritize the refinement of mathematical processes and result optimization. Orbital Determination (OD) uses the result from IOD techniques as an initial approximation of an object's orbital parameters and aims to refine the accuracy of those results. Often, IOD is used to expedite the OD process, offering an initial estimation closer to the actual orbital parameter values of a detected object compared to a random guess. The IOD initial estimation allows for optimizers to converge to a result faster than starting with a random guess [10].

Table 2.1: Angles-only Initial Orbit Determination Methods

IOD METHOD	INPUT INFORMATION	SUMMARY
Laplace's Method	• Angular measurements and times which can be obtained from different sites at different times [11] • Observer's position at the same times	• First created to estimate middle position and velocity vectors in a group of observational data for the orbits of comets and minor planets [11] • Works poorly for near-Earth satellites [11]
Gauss's Technique	• Angular measurements and times with limited spread of data. Ideally less than 60 degrees apart [12] • Observer's position at the same times • Works best when data is separated by 10 degrees or less i.e. 5-10 minutes apart for low-Earth Satellites [11]	• Assumes the three position vectors lie in a single plane [11] • Fits more scenarios than Laplace's Method [11] • Modestly robust [11] • Best suited for differential-correction techniques [11] • Low order approximation of Lagrange Series [12]
Double-R Iteration	• Angular measurements for larger spreads of data i.e. bigger differences in times and locations of observations [11] • Observer's position at the same times	• Good for general applications [11] • Suited for multi-site observations where data points are far apart. [11] • Doesn't work well with observations that have low angular separations [11]
Goodings	• Angular measurements and times [11] • Observer's position at the same times • Can handle data from multiple revolutions [11]	• Similar to Double-R Iteration [11] • Robust approach for general applications; used commercially [11] • Challenge is ensuring all parameters are set correctly and determining which solution is correct [11]

2.1.3: RSO Identification and Correlation

In the field of Space Situational Awareness (SSA), RSO identification plays a vital role in tracking space assets and debris. Space assets and debris are catalogued by USSPACECOM and assigned a satellite number known as NORAD ID, along with TLE information [13]. This cataloguing system serves to manage congestion that is caused by space debris and contributes to

SSA [13]. Centralized catalogs allow for tracking and updating TLEs in order to track and protect space assets and debris. TLEs contain important orbital information and are associated with a unique satellite number formatted as shown below [14][15]:

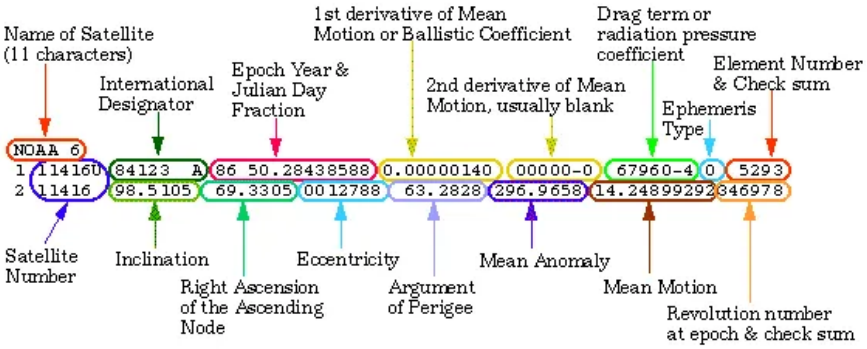

Figure 2.1: TLE Orbital Information Outline

RSO catalogs containing orbital information serve as a cross reference point that connects collected data from SSA research to existing knowledge about the RSO population. Various systems and approaches exist for correlating observed RSOs with their identities and update RSO databases. One existing system called Catalogue Maintainer Software (*catmai*) is an automated process that encompasses IOD, OD, and identity correlations to establish and maintain space object catalogues [16]. The *catmai* system accepts images from various sensors and, through synthetic track generation and comparisons in the measurements domain, strives to correlate the observed objects to their existing counterparts in the catalog, when possible [16]. Unlike some existing methods which typically use IOD and OD for orbit domain correlations, *catmai* uses IOD and OD techniques to update the catalog's orbital information after performing the correlation in the measurement domain [16] Additionally, C-CORE has developed an algorithm which uses optical observations of an RSO and data from the USSPACECOM TLE database to correlate the identities of the observed objects. C-CORE's method involves the application of orbital propagation techniques, orthographic projection, and TLE data to correlate

observed tracks to propagated tracks. Similar to catmai, C-CORE conducts their comparison in a measurement domain by comparing observed pixel locations in the images against those propagated based on TLE information. In conclusion, RSO identity correlation is a powerful and crucial part of SSA research for maintaining and protecting space assets and debris.

2.2: Space-based vs Ground-based Images of RSOs

Capturing optical images of RSOs from both ground-based and space-based observers offers different advantages and disadvantages, each tailored to specific requirements and applications. Space-based observations offer a range of advantages, such as immunity to weather conditions and minimal limitations due to Sun/daylight interference. These observers tend to have smaller apertures which can reduce their image sensitivity [17]. Incorporating larger aperture sensors in space-based platforms enhances sensitivity, although at the expense of increased complexity and cost. The deployment of space-based observers in LEO is comparatively economical and benefits from a more benign radiation environment [17]. Nonetheless, the challenge of dealing with Earth blockage arises in LEO orbits and must be addressed [17]. To mitigate the added congestion from new technologies being launched into Earth's orbits for SSA research, one approach is repurposing existing optical sensors already in orbit, such as star trackers [18]. Another potential drawback of space-based sensors is their vulnerability to anti satellite (ASAT) actions that could cause significant setbacks and incur substantial costs [17]. This lack of resilience, combined with data limitations, further complicates the intricate balance between the advantages and disadvantages of space-based observers.

Conversely, ground-based observations hold their own set of advantages and drawbacks. This approach offers cost-effective alternatives, ranging from amateur to professional telescopes, accommodating diverse complexities. Ground-based observers can feature relatively

larger apertures compared to space-based instruments, which enhances their sensitivity. However, it is important to note that larger telescopes correspondingly entail higher expenses. Meanwhile, smaller ground-based telescopes provide a cost-efficient solution, allowing easier deployment in remote locations [17]. Nonetheless, a global distribution of ground-based instruments is necessary to achieve comprehensive sky coverage and maximize RSO observations [17]. Ultimately, the choice between ground-based and space-based observations depends on a variety of factors, such as cost, sensitivity, resilience, and coverage requirements. The suitability of either method varies based on the specific needs of the applications at hand.

2.3: Image Processing: Noise Filters & Edge Detectors

2.3.1: Noise Filters

In the context of image processing, noise can disrupt the integrity of visual data, introducing artifacts and compromising the accuracy of image analysis. Image noise reduction is standard part of pre-processing in image processing pipelines [19]. Noise filtering is used to remove or reduce the amount of noise in an image while still preserving essential details and information. There are various filters, each with its own challenges, methods, domains, and ideal applications. Noise reduction filters can exist in both spatial and frequency domains and can employ linear, non-linear, and adaptive approaches. Spatial linear filters, such as the Gaussian smoothing filter, blur the image using a Gaussian function but may simultaneously reduce both noise and image details [19]. Other filters, such as the mean and median filters, use a sliding window to replace the pixel value at the center of the window with the mean or median value of the surrounding pixels to smooth the image [19]. One of the key distinctions between the mean and the median filters is their linearity, which characterizes the properties and behavior of a filter. Linear filters like the mean filter tend to follow fundamental properties such as the

superposition principle and shift invariance along with causality and stability conditions [20]. On the other hand, non-linear filters like the median filter can produce non-intuitive outputs that do not follow these conditions, particularly shift and scale invariance [20].

Another example of a linear filter is the Wiener Filter, which is a Mean Square Error (MSE) optimal low pass filter [21]. Linear filters, such as the Wiener filter, can be implemented with an adaptive approach in which the local standard deviation can influence the amount of smoothing applied [22]. This approach allows for locally optimized smoothing and helps in preserving edges in the image [22]. Each of these approaches has its own advantages and performs optimally on different types of noise. For instance, Median filters are effective when dealing with salt and pepper noise, and they maintain edges well, while Mean filters are suitable for Poisson noise but may over-smooth edges [19]. Dealing with noise in images offers various approaches and selecting the optimal method can be a challenging task. A thorough understanding of the images and their unique challenges can guide the selection of the most suitable approach for noise reduction during the preprocessing phase.

2.3.2: Edge Detectors

Edge detection is a fundamental technique in image processing used to identify boundaries in different areas of an image. Edge detectors are designed to locate regions with rapid local changes in the image's intensity, essentially high-frequency areas. There are several edge detection techniques available, including Sobel, Prewitt, Laplacian, and Canny Edge detectors. Each edge detection technique has their own advantages, methods, and applications. Edge detectors generally follow three main steps, enhancement, detection, and localization [23]. 'Edges' are typically defined by rapid changes in intensity within a local area of the image. During enhancement, these regions of local change are emphasized, often by computing the

gradient magnitude of the area [23]. Intuitively, the detection step focuses on identifying strong edges present in the image [23]. Detection is followed by localization where if needed, the subpixel location and orientation of the edge can be determined [23]. The Sobel filter is a widely used technique that leverages differentiation and smoothing using small convolutional filters. These 3x3 convolution masks are shown below:

$s_x =$

-1	0	1
-2	0	2
-1	0	1

$s_y =$

1	2	1
0	0	0
-1	-2	-1

2.1

The gradient components obtained from applying these kernels to an input image are used to calculate the gradient magnitude and angle of edge orientation, as given by the equations [24]:

$$|G| = \sqrt{G_x^2 + G_y^2} \tag{2.2}$$

$$\theta = arctan(G_y \,/\, G_x) \tag{2.3}$$

The Prewitt filter uses a similar approach and equations but uses a slightly different kernel, as shown below [23]:

$s_x =$

-1	0	1
-1	0	1
-1	0	1

$s_y =$

1	1	1
0	0	0
-1	-1	-1

2.4

Another commonly used filter is the Laplacian Operator which uses the following formula to calculate the two-dimensional equivalent of a second derivative [23][25]:

$$\nabla^2 f = \frac{\partial^2 f}{\partial x^2} + \frac{\partial^2 f}{\partial y^2} \qquad \text{or} \qquad \Delta f = \sqrt{\frac{\partial^2 f}{\partial x^2} + \frac{\partial^2 f}{\partial y^2}} \tag{2.5}$$

In this edge detection approach, edges are detected where the second derivative is equal to zero, at a point of maximum intensity [25]. The Laplacian operator differs from the other filters in that it only uses one kernel. This method also benefits from Gaussian smoothing at the beginning due to its sensitivity to noise [26].

The Canny edge detector is another popular algorithm for edge detection due to its high accuracy and lower susceptibility to noise. It identifies edges through a multi-stage process which includes smoothing the image using a Gaussian filter, computing the gradient magnitude and orientation, applying non-maximum suppression, and applying hysteresis thresholding. While this process can be complex, it aids in the identification of strong, thin, and continuous edges while supressing noise and false edges. The Canny filter starts by convolving an image with a Gaussian filter to smooth it. Similar to previous edge detection approaches, Canny then performs gradient calculation in both horizontal and vertical directions to detect potential edges. A Sobel filter can be used to perform this gradient calculation while equations 2.2 and 2.3 can be used to calculate the magnitude and direction. Following these gradient calculations, non-maximum suppression is used to thin out detected edges. Finally, a double threshold step is applied to identify which edges are strong, weak, and non-relevant to refine the detected edges by reducing false edges [23][27]. Thresholding an image with hysteresis refers to using both an upper and lower threshold, addressing issues of false edges from setting thresholds too low and gaps in the edges (i.e. false negatives) from setting thresholds too high [23][25]. The robustness introduced from these various steps for edge detection makes the Canny filter a widely used approach. Edge detectors are powerful tools for extracting features of interest from images, with each approach having its own advantages and disadvantages, ranging from complexity to robustness.

Chapter 3: Image Databases

3.1: Introduction

The choice of image database is an important aspect in performing image processing research. The selection of appropriate datasets ensures that the performance of the image classification algorithm and initial orbit determination algorithm is evaluated thoroughly and accurately. Image databases encompass a wide range of diversity and complexity, necessitating researchers to carefully consider their specific research objectives when making their selection. By choosing the appropriate image datasets, researchers can effectively assess the capabilities and limitations of their algorithms, as well as evaluate their performance in diverse real-world scenarios.

This chapter focuses on the various image databases employed in the present study, shedding light on their distinctive properties and the rationale behind their selection. A comprehensive evaluation of the proposed algorithms necessitated the inclusion of datasets that effectively represented the challenges and variations encountered in practical applications. The selected image databases were tailored to cover a broad spectrum of relevant scenarios, ensuring the algorithms were rigorously tested across different conditions. The chapter delves into the characteristics of each dataset, including their resolution, image quality, object diversity, and environmental conditions.

3.2: Starlink Field Campaign Images

The Starlink field campaign images were captured by a research assistant in the Nanosatellite Lab at York University. The images were captured north of Toronto, in Blue Mountains, Ontario to reduce the effects of light pollution. The imaging process involved

mounting a ZWO ASI183 Pro scientific camera with a 1″ CMOS IMX183CLK-J/CQJ-J sensor onto an amateur telescope with a focal length of 1200mm [28]. This particular dataset, although small, played a crucial role in the initial development of a classification tool. The utilization of an amateur telescope in conjunction with a scientific camera resulted in a narrow, zoomed-in field of view for capturing the images. The primary objective of capturing these images was to target Starlink satellites; however, the specific identities of the photographed resident space objects (RSOs) remain unconfirmed. Nevertheless, these images were exceptionally suitable for the initial development phase due to their limited quantity, which expedited the process of manual labeling. The streaks captured in the images were clearly visible and substantial, making them easily detectable by the early versions of the classification tool. Figure 3.1 illustrates an example of a streak detected in this data set. Notably, the resolution of these images was set at 5496 x 3672 pixels, and they were captured with an exposure time of 300ms.

Figure 3.1: Streaking RSO in Image

3.3: Torrance 2021 Field Campaign Images

The Torrance 2021 field campaign images used in this research were captured by team of researchers from the Nanosatellite Lab at York University for Space Situational Awareness research. To ensure optimal conditions for observing potential RSOs, the field campaign was conducted in Torrance, Ontario, situated north of Toronto. This location was carefully chosen to minimize the adverse effects of light pollution emanating from the city and to maximize the visibility of RSOs against the night sky. During the field campaign, a team of researchers set up a pco.panda 4.2 camera with a ZEISS Dimension 2/25 lens on a stable tripod. Throughout the night, the camera captured a series of images with the primary objective of photographing RSOs. To enhance the likelihood of capturing RSOs, the team relied on the Heavens Above website, which provided accurate predictions of RSO passings over the observation area [29]. This information allowed researchers to strategically position and orient the camera, maximizing the chances of capturing RSOs within the frame. The images had a resolution of 2048 x 2032 and were time stamped on the top left corner. To ensure optimal visibility of the RSOs against the starfield background, the images were captured using exposure times ranging from 3 to 5 seconds. This longer exposure duration facilitated the capture of RSOs as distinct bright streaks against the darkened backdrop of the starry sky. An illustrative example of an RSO streak detected within an image sequence from this specific dataset is depicted in Figure 3.2. These field campaign images proved to be highly valuable for the development of an image classification algorithm. The elongated streaks resulting from the longer exposure times, coupled with the contrasting dark background, significantly facilitated the detection of RSOs. This dataset provided an excellent basis for algorithm refinement and fine-tuning, enabling the algorithm to better detect and classify RSO streaks in image sequences.

Figure 3.2: RSO Streak in Field Campaign Sequence

3.4: Resident Space Object Near-space Astrometric Research (RSONAR) Images

The Resident Space Object Near-space Astrometric Research (RSONAR) mission was flown on the STRATOS balloon that was launched by the Canadian Space Agency (CSA) in Timmins, Ontario on August 2022 [30]. The STRATOS balloon program is designed to facilitate research and validate new technologies by launching a stratospheric balloon with a payload containing the scientific projects to near space [30]. The RSONAR imager was designed by a team of researchers from the Nanosatellite Lab at York University [31]. The RSONAR mission demonstrated the use of a commercial-grade star tracker for SSA work by capturing images of RSOs from the stratosphere [31]. The primary objective was to capture images of RSOs from the stratosphere using a wide Field of View (FOV) camera with low resolution, similar to a star tracker. The payload, consisting of off-the-shelf hardware, successfully operated at an altitude of

approximately 40 km, capturing images during the night portion of the flight. By adjusting camera parameters based on altitude data obtained from a GPS sensor, the mission aimed to maximize the number of high-quality images taken during optimal observation conditions.

The payload's optical system was equipped with a pco.panda 4.2 camera and a ZEISS Dimension 2/25 lens, providing a wide FOV of 29.7 degrees [31]. The camera sensor had a maximum resolution of 2048 x 2048 pixels. The images used for the image classification were mainly captured with an exposure time of 100ms but could be varied and adjusted if necessary. In some images, the RSOs appeared as bright points in the image and needed to be stacked for RSOs to appear as streaks. Figure 3.3 illustrates an example of a stacked image where the RSOs stacked into streaks. Meanwhile, in other images, objects appeared as streaks in a single image frame. Figure 3.4 illustrates an example of a streak captured in a single image. Out of the total 93,000 images captured during the RSONAR mission, the initial 5,400 images taken during ascension were deemed less valuable for analysis. These images were captured during an unstable portion of the flight and were unlikely to contain any RSOs. Hence, they were discarded from further consideration. Although the images after the initial ascent were more stable, images with some sway where the stars streaked were still present but not unmanageable. From the remaining images, a subset of 2,700 was selected for manual labeling, specifically for the purpose of streak detection algorithm testing and verification. The entire dataset served to be extremely useful for SSA research within the Nanosatellite Lab and contributed to research including object detection using machine learning, image classification, and RSO identification research.

Figure 3.3: Stacked Image Sequence with Streak from RSONAR Mission

Figure 3.4: Single Image from RSONAR Mission Containing a Streak

3.5: NEOSSat Images

The Near-Earth Object Surveillance Satellite (NEOSSat) is a Canadian microsatellite designed to search for near-Earth asteroids and track space debris in orbit around the Earth [32]. In addition to its primary mission, NEOSSat has also been used to observe other satellites in orbit around the Earth. NEOSSat is tasked by the Defence Research and Development Canada (DRDC) to perform observations of RSOs under the High Earth Orbit Space Surveillance (HEOSS) project. The satellite uses its onboard telescope to image the space around it and detect other objects in orbit. This capability has been used to study the distribution of satellites and debris in orbit and to detect and track new objects. The observations from NEOSSat have contributed to a better understanding of the space environment around the Earth and have helped to improve space situational awareness.

NEOSSat is equipped with a Maksutov optical telescope that has a 15 cm aperture and a focal length of 1.8 meters [33]. The telescope has a field of view of 1.5 degrees and an angular resolution of 3 arcsecond/pixel [33]. NEOSSat operates in a sun-synchronous orbit at an altitude of approximately 800 km, which provides a clear view of the entire sky. This microsatellite captures images in the visible and near-infrared spectrum and has a data storage capacity of up to 32 GB [33]. The captured images are transmitted to the ground station for analysis and processing. The sensor specifications and capture parameters of NEOSSat have been optimized for different research applications, including the detection and tracking of satellites and debris in orbit around the Earth.

Due to the large range of applications for NEOSSat's images, its database is vast and diverse. This research focused on optical images captured by the satellite. The images tasked by DRDC to observe RSOs are typically done in track rate mode (TRM). TRM tracks the RSO

being observed so it appears as a single dot while the stars appear as streaks in the background. Because this research focuses on streak detection, these pictures were not used for the image classification algorithm. Instead, images in ‘stare’ mode where the camera remained pointed at one part of the sky and the stars appear as singular dots while moving objects such as comets, asteroids, and potential RSOs may appear as streaks depending on exposure time. Figure 3.5 illustrates an example of a streaking object over a starfield from this database.

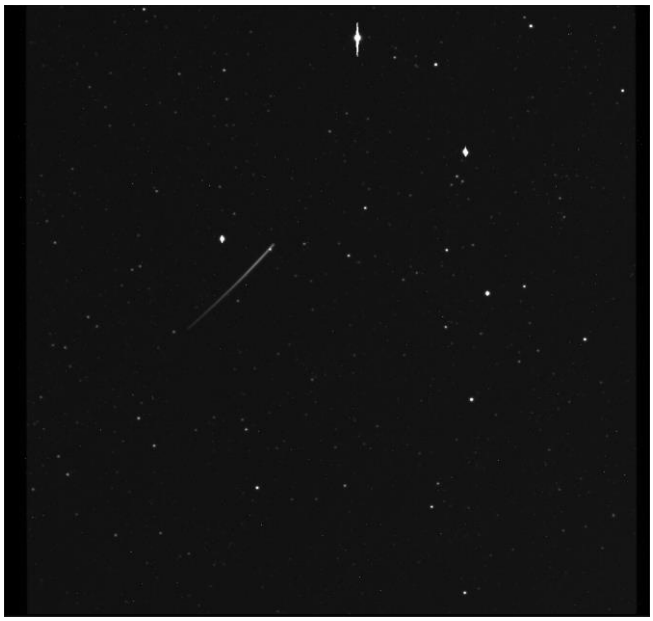

Figure 3.5: NEOSSat Image Containing a Streak

NEOSSat images also posed their own unique challenges. Some images had bright stars which saturated pixels and overflowed to create an artifact that made them appear as long streaks with a bright center. Figure 3.6 shows an example of two stars which oversaturated the pixels. The effects of these pictures and how they could be addressed in the future for image classification will be discussed further in Chapter 4. The NEOSSat database was one of the more comprehensive image databases looked at. It contained calibration frames for optical images which can be used for improving object detection algorithms by compensating for distortions

from the hardware itself. In addition, the database contained images with noise from interference from the hardware itself but also contained the clear counterparts to those images with those frequencies removed. These cleaned up images were removed of that noise and labeled as ‘clean’. Overall, NEOSSat images, though challenging to navigate through, were more comprehensive and better geared for complex image processing research than other datasets.

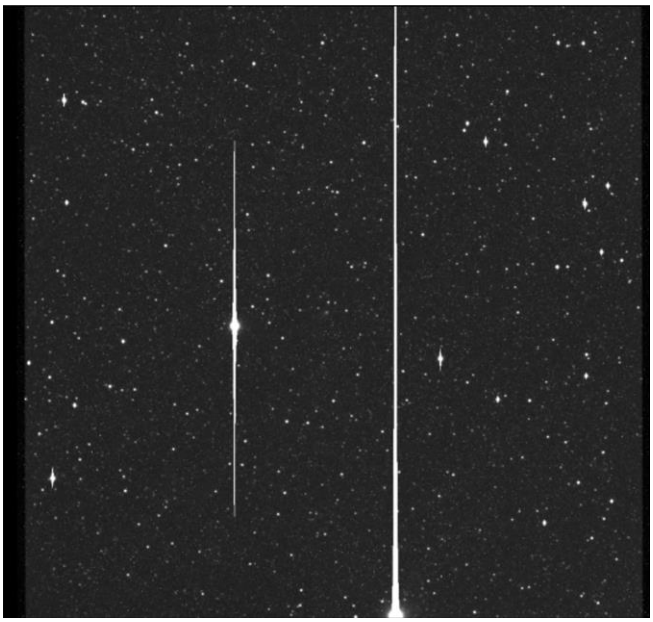

Figure 3.6: Images Containing an Over-Saturated Star Pixel

3.6: CASSIOPE Fast Auroral Imager (FAI) Images

The Fast Auroral Imager (FAI) instrument is a crucial component of the Cascade SmallSat and Ionospheric Polar Explorer (CASSIOPE) spacecraft, specifically designed to capture high-resolution imagery of auroral emissions within Earth's atmosphere [34]. The FAI instrument is equipped with two charged-couple device (CCD) cameras to detect near infrared (650-1100nm) and visible (630nm) light emitted by the aurora [35]. The near-infrared images are obtained at an exposure rate of 0.1 seconds per second, while the 630nm images are captured at an exposure interval of 0.5 seconds every 30 seconds [35]. In addition to its primary mission

objectives, the FAI cameras have proven instrumental in the imaging and detection of space debris in orbit, contributing significantly to SSA research and debris mitigation efforts. Leveraging the FAI's observational capabilities for satellites and space debris, CASSIOPE extends its scientific reach, fostering a deeper understanding of the intricate space environment enveloping our planet. Notably, the imagery acquired in the 650-1100nm wavelength range serves as a valuable resource for SSA research purposes, closely resembling images obtained from low-resolution cameras [36]. An example of a near-infrared image can be seen in Figure 3.7 with a few objects clearly visible within the field of view.

Figure 3.7: FAI Image with Some Visible Objects

Moreover, the FAI imagery has been instrumental in the development of obstruction detection techniques, utilizing Earth's limb presence in some images. Figure 3.8 illustrates an example of an image in which the Earth’s limb is obstructing part of the field of view.

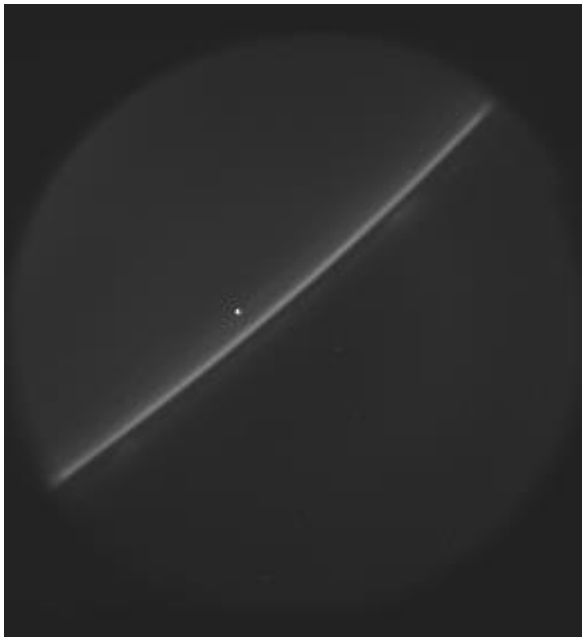

Figure 3.8: FAI Images with Earth's Limb Obstructing the FOV

The FAI imagery presented distinctive challenges that set it apart from other data sets. One challenge involved the shape of the captured image, which appeared as a circular structure against a black square background. This characteristic required specific attention and processing techniques to ensure accurate interpretation and analysis. Another significant hurdle arose from the presence of glares on the camera lens resulting from external light sources. These glares posed difficulties in discerning objects within the field of view, including stars and RSOs thereby demanding meticulous efforts to overcome the glare and extract valuable information. The comprehensive database containing the FAI images is readily accessible on the ePOP website, offering a wealth of data for researchers.

3.7: Space-Based Optical Image Simulator (SBOIS): Simulated FAI Images

The Space-Based Optical Image Simulator (SBOIS) is a MATLAB program developed by a former member of the Nanosatellite Research Lab at York University. Its main goal is to

create annotated images from space-borne imagers for training AI algorithms in SSA research [36]. The SBOIS Simulator performs all calculations required to simulate the optical environment such as combinations of direct and reflected flux from sources like stars, Earth, Earth's Limb, Earth's Moon, Sun, and Zodiac [36]. It assumes RSOs are not active sources but reflectors of solar radiation [36]. The simulator accounts for active sources like the Sun and stars as point sources and calculates their magnitude to Digital Number (DN) values using specific equations [36]. For area sources like Earth and others, surface brightness is used to calculate DN values. The simulator incorporates parallel processing to reduce computation time and handle the simulation of thousands of moving RSOs efficiently [36]. SBOIS utilizes parallel processing with SIMD to reduce computation time, and the Parallel Specialized Perturbation Method 4 (PSGP4) Propagator for efficient RSO propagation [36]. Moreover, the simulated images used in this research were based on the sensor parameters on CASSIOPE's FAI hardware during different scenarios. Therefore, these images had a resolution of 256x256 pixels with an exposure time of 0.1s. The simulated images included objects that would be seen within FAI's FOV during specific observation scenarios. These objects included RSOs, stars, and Earth's Limb if applicable. Figure 3.9 showcases an example of a simulated image with Earth's limb in the FOV along with some auxiliary information in the title [36]. As previously mentioned, the SBOIS images were particularly useful as they were labeled with information on the visible objects. The information included auxiliary data such as coordinate rotation matrices, object brightness, labeled star locations, and essential information about the RSOs [36]. The labeled images served as truth data for the development and initial testing of the IOD algorithm.

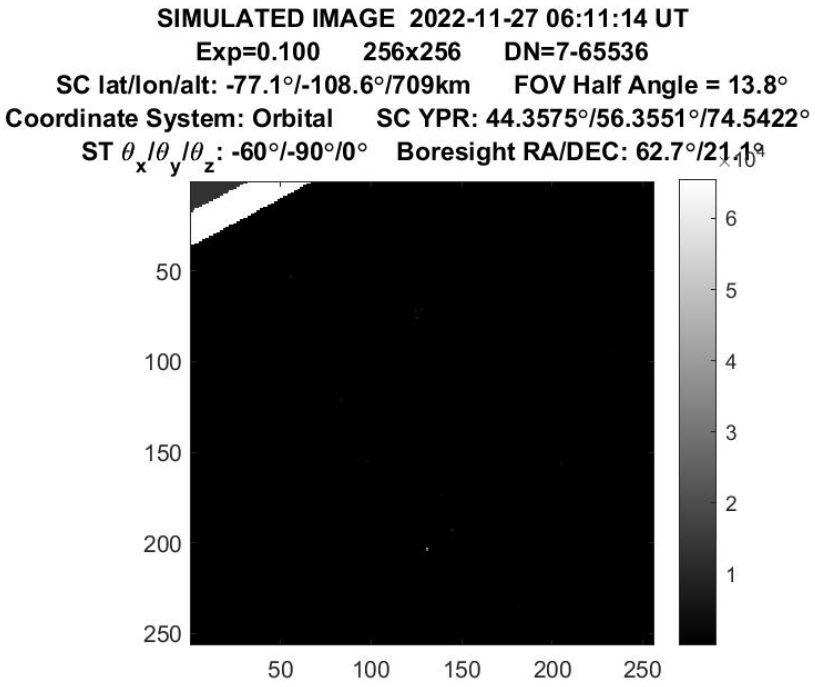

Figure 3.9: Simulated Image of the FAI image with Auxiliary Information

3.8: Summary of Camera Parameters and Features

The datasets examined in this study demonstrate the wide diversity and complexity inherent in image databases used for image processing research. Each dataset serves a distinct purpose, addressing specific research objectives and challenges encountered in the realm of SSA research. Understanding and leveraging the distinctive challenges posed by each dataset proves instrumental in testing various aspects of applications and assessing the robustness of SSA algorithms. The selection of appropriate datasets is crucial for the development of SSA algorithms and for the evaluation of their performance in practical applications.

Understanding the sensor parameters, image capture conditions, features, available information, and challenges of each dataset is crucial for choosing the most suitable dataset for different applications. Table 3.1 provides a clear summary outlining different camera sensor parameters and features that were explored and studied across the datasets in this study

[28][31][33][34][35][36][37][38]. These parameters include whether the dataset includes images captured in stare mode, tracking mode, or a combination of both. In stare mode, the camera remains in a fixed or relatively stationary position throughout image capture. In this mode, the imager captures images of a specific region of the sky over an extended period. Depending on exposure duration, objects like RSOs may appear as singular point sources in short exposures or streaks in longer exposures. On the other hand, track mode involves the camera actively following an object's movement across the sky, resulting in the object of interest appearing as a singular point while stars create streaks in the background.

Another parameter documented in table 3.1 pertains to the pixel scale derived from the sensors within each respective database. Calculated using equation 3.1, this parameter shows an inversely proportional relationship between pixel scale and focal length [39]. Correspondingly, with an increase in pixel size, the pixel scale exhibits a proportional change. Pixel scale is significant due to its influence on image sensitivity and the extent of details resolved in an image. This metric indicates the angular span covered by a single pixel across the celestial canvas. An optimal pixel scale would allow for images that are neither oversampled nor under sampled which affects the quality of the acquired data. A higher pixel scale, indicative of oversampling, spreads starlight across multiple pixels, reducing the sensitivity of the image [40]. Meanwhile, lower pixel scales can result in under sampling of the image where the stars can appear blocky and some of the light from the background can merge with light from a star in a single pixel.

$$pixel\ scale = \frac{206.265 * pixel\ size\ (\mu m)}{focal\ length\ (mm)} \qquad 3.1$$

Table 3.1: Summary of Image Database Parameters

	Starlink Observations	Torrance 2021 Campaign	RSONAR	NEOSSat	CASSIOPE's FAI: 650-1100nm	Simulated FAI
Observer Location	Ground	Ground	Near-Space	Space	Space	Simulated Space
Resolution	5496 x 3672	2048 x 2032	1024 x 1024	Varies with maximum 1024 x 1024	256 x 256	256 x 256
Exposure	300ms	3-5s	100ms	Varies	0.1s	0.1s
FOV (degrees)	~1.031	29.7	29.7	0.85	26	26
Pixel Size (µm)	2.4 x 2.4	6.5 x 6.5	6.5 x 6.5	13 x 13	26 x 26	Simulated 26x26
Focal Length	1200mm	25mm	25mm	893mm	68.9mm	Simulated 68.9mm
Pixel Scale (arcseconds/ pixel)	0.41	53.6	53.6	3	77.8	Simulated 77.8
File Type	PNG	tif	tif	FITS	FITS	mat
# of Testing Images	43	917	2,700	82+	20+	233
# of Database Images	43	917	93,000+	Several Thousand	Several Thousand	N/A
Pointing Settings Available	Stare Mode	Stare Mode	Stare Mode	Stare Mode/Track Mode	Stare Mode	Stare Mode
Source	Nanosatellite Lab, York U	Nanosatellite Lab, York U	Nanosatellite Lab aboard STRATOS balloon	NEOSSAT Mission, CSA & DRDC	CASSIOPE Mission, University of Calgary	SBOIS Simulator
Role in this research	Image Classification Development	Image Classification Development	Image Classification Testing	Image Classification Testing	Image Classification Development and IOD Future Work	IOD Testing

Utilizing insights drawn from each dataset, informed decisions can be made regarding the most suitable datasets for various SSA applications. The Starlink Field Campaign Images dataset, despite its small size, played a vital role in the initial development of the classification tool. The narrow field of view resulting from the amateur telescope and scientific camera enabled easy detection of streaks, expediting the manual labeling process. Conversely, the Torrance 2021 Field Campaign Images dataset provided a larger number of images with longer exposure times, offering elongated streaks against a dark background. This setup was ideal for testing and refining the image classification algorithm.

The NEOSSat image dataset offered a comprehensive and extensive database with various research applications, including the detection and tracking of satellites and debris. The dataset provided images of moving objects against a stationary starfield background, making it suitable for researching streak detection. It also contained images in tracking mode, which could be utilized for other research such as light curve analysis. Additionally, the dataset included calibration and noisier images, which can be used for studying noise reduction techniques and more advanced image processing methods.

Meanwhile, RSONAR images provided a unique opportunity for SSA research stemming from their capture via a high-altitude balloon in the stratosphere. RSONAR effectively demonstrated the ability to observe RSOs for SSA research using readily available hardware in a near-space environment. This dataset proved valuable for testing the detection of streaks that were created by stacking a sequence of short exposure images.

The FAI image database offered the opportunity to test image processing methodologies on lower resolution images in a space-based environment. These images had unique challenges such as the presence of Earth’s limb in the field of view and instances of pronounced lens glares.

These scenarios offered opportunities to test and develop new techniques such as obstruction detection. Additionally, the images in this database facilitated a constructive comparison with simulated FAI images to offer examples of real vs simulated image performance. The simulated FAI images had the great advantage of containing labeled information ideal for testing algorithms and training machine learning programs. Ultimately, each dataset contributed significantly to this study, offering distinct insights and challenges that propelled advancements across various parts of SSA research.

Chapter 4: Image Classification

4.1: Introduction

The image classification algorithm was originally developed to sort images captured from the RSONAR mission. Its development commenced prior to the deployment of the RSONAR payload and was initially developed and tested with other databases. With over 93,000 images produced from the mission, manual inspection would have demanded substantial resources. The primary objective of this classification tool was to identify image sequences containing resident space object (RSO) streaks, aligning with the RSONAR mission's goals.

To optimize computational efficiency, the algorithm focused on bulk image processing rather than individual image processing in most databases. Bulk processing through image stacking also enabled the detection of RSOs from short exposure images along with streaks from long exposure images. Through the process of image stacking, RSOs from short exposure images combine to create an RSO 'streak'. Additionally, an obstruction detection feature was introduced to identify images which displayed non-RSO signals such as the Earth's limb or the moon. This added feature did not apply to the RSONAR mission as none of those images contained obstructions. The classification pipeline, illustrated in Figure 4.1, employed various image processing techniques to categorize image sequences from diverse datasets.

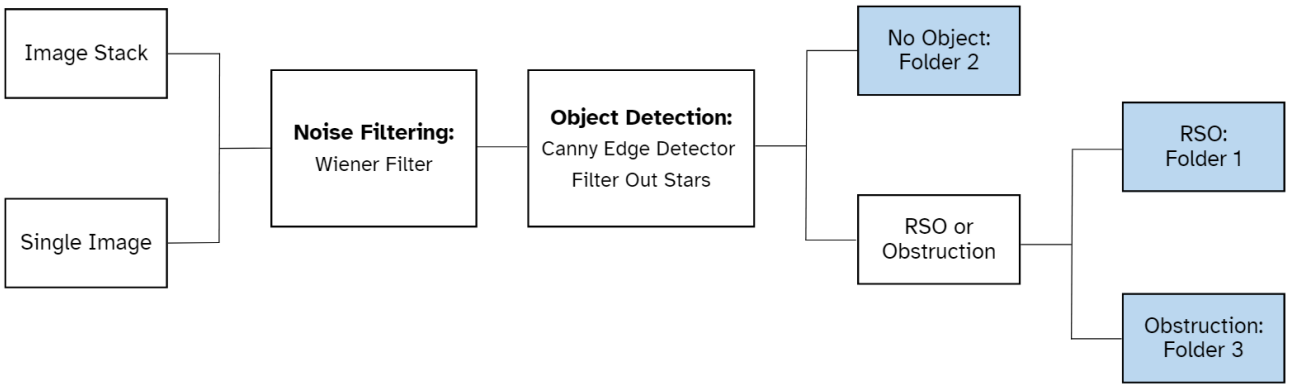

Figure 4.1: Image Classification Pipeline

4.2: Classification Methodology

4.2.1: Preprocessing

The classification algorithm starts with a preparatory phase prior to analysis. In this pre-processing stage, the image data is prepared by addressing any issues such as noise and applying any special processes required for the analysis. When applicable, images are first converted from RGB to grayscale and processed in double precision. The image sequence input into the classification algorithm is stacked using weighted addition. The weights applied to each image are contingent on the sequence's image count. Using image stacking, the algorithm saves on computation time through bulk processing. Noise filters and edge detectors are later applied to the stacked image, avoiding the need for processing each individual image separately. Stacking also enables the detection of single point source objects by forming a streak using high-frequency image captures. The high frequency capture maintains continuity in the stacked streak, ensuring no gaps between points. Figures 15 and 16 demonstrate the output of the stacking process on Starlink Observations and RSONAR image sequences. Notably, the RSONAR sequence exhibits point-source RSO images that were stacked to create a streak. The discontinuities seen in the stacked streak were a result of delays between some image capture.

Meanwhile, the Starlink Observation image shown is a group of 5 images each containing a streak that were combined to form one large streak. As the streaks might be difficult to see, adjustments were made for clarity in the figures. The image in Figure 4.2 has been cropped to enhance the streak's visibility, while Figure 4.3's second photo was inverted for better viewing.

Figure 4.2: Starlink Stack of 5 Images

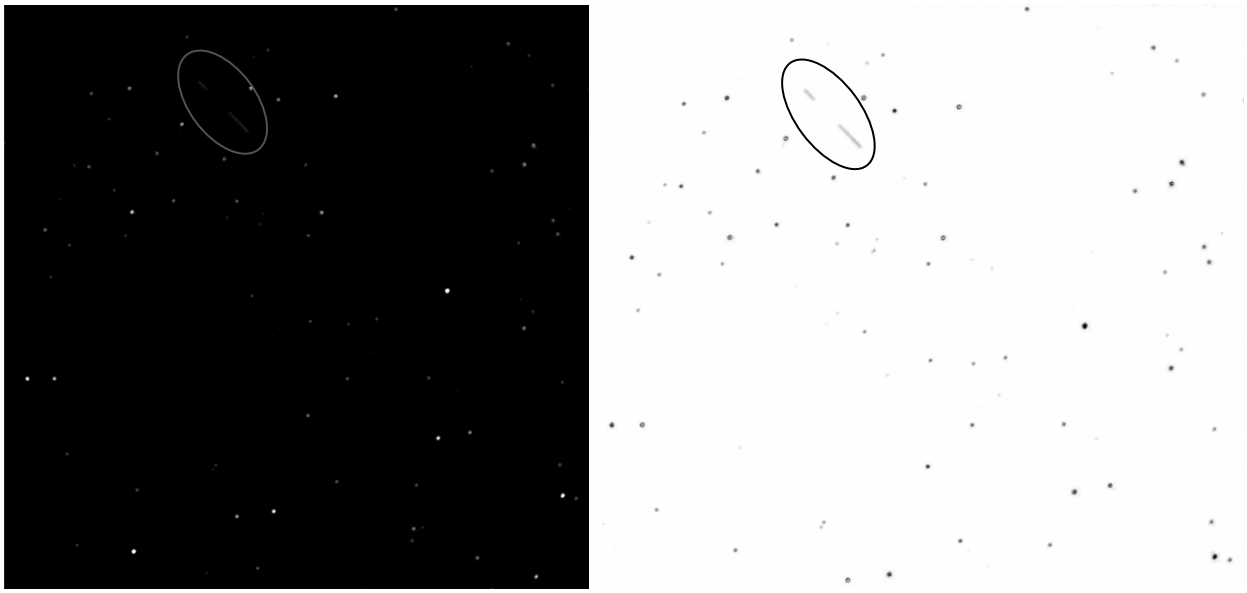

Figure 4.3: RSONAR Stack of 27 Images and Inverted for Viewing

The NEOSSat images differed from other databases as they were individually processed without stacking. They were unique in that different image tracks had varying resolutions, making it unfeasible to stack an entire subset without binning due to differing image sizes. Binning for standardizing resolutions was considered, but the decision was made to maintain original image sizes and process them individually. The decision to avoid binning was rooted in the understanding that it would result in the loss of crucial information and details, potentially causing the overlooking of dim objects during the object detection phase.

Subsequently, the next preprocessing step aims to reduce noise in the stacked image. Different databases exhibit diverse noise levels influenced by factors such as sensor types and environmental conditions, including light pollution and temperature fluctuations. Locally adaptive filters such as the Wiener filter are instrumental for tackling varying noise levels throughout an image [41][42]. This filter is particularly useful due to its ability to simultaneously deblur and denoise, maintaining edge information. The Wiener filter is useful in scenarios where some restoration due to motion blur is required [42]. The adjustment of the Wiener filtering window size is tailored according to the image's resolution.

Additionally, it is essential to note that unique challenges arose from each dataset that required resolution prior to the noise filtering step in the preprocessing stage. For instance, the Torrance 2021 Field Campaign images contained a time stamp at the top left of each image, obstructing the image. The classification tool identified the time stamp as an obstruction as it appeared in the same area in all images. To address this, the area of pixels containing the timestamp was excluded from further processing. The RSONAR images presented a significant noise challenge in each image. Stacking introduced additive noise that hindered the detection of fainter objects and led to multiple false detections. To address this issue, the RSONAR database

was filtered using the Wiener Filter before stacking the image sequence. Moreover, the RSONAR datasets contained empty files that couldn't be opened because no information existed within them. The classification tool was modified to detect and disregard these files. Other unique challenges encountered across the databases involved checking and removing images with zero intensities or those that were incomplete.

4.2.2: Object Detection

Following the preprocessing phase, the image proceeds to the object detection phase of the classification process. In this stage, the algorithm employs an edge detector to identify gradient changes within the images, aiming to detect RSO streaks. The Canny filter was selected for its robustness and ability to detect faint edges, owing to its hysteresis thresholding. During testing in the development phase, this edge detector effectively detected RSO streaks and outperformed other filters like the Sobel filter. The Canny filter outputs an image with only the detected edge pixels as illustrated in Figure 4.4.

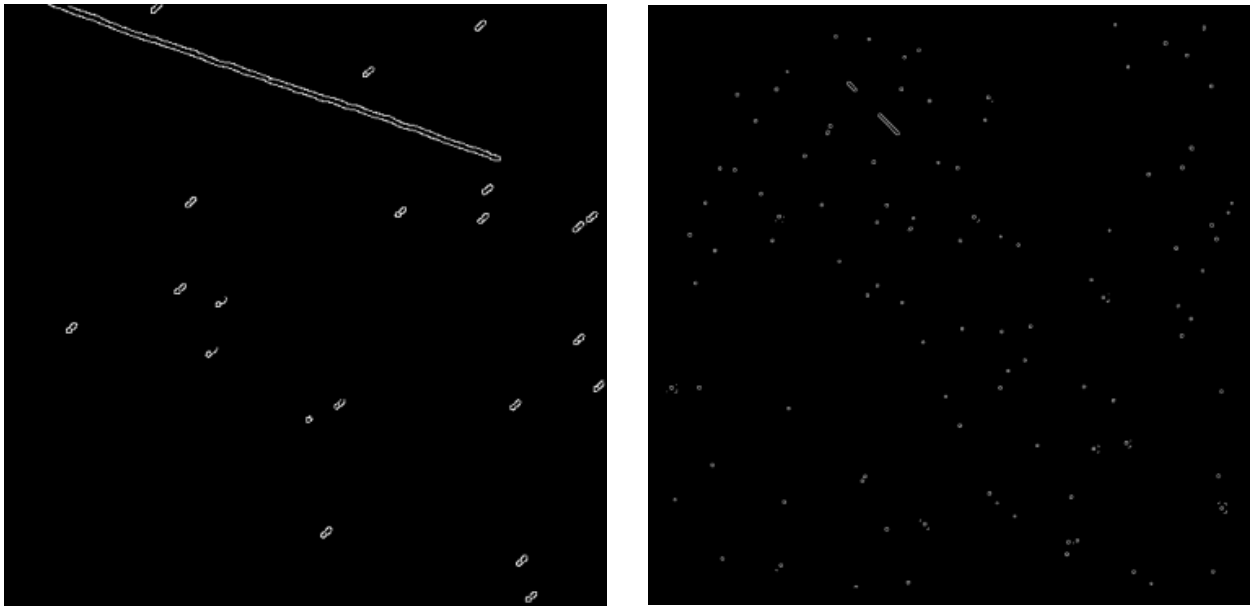

Figure 4.4: Canny edge detection output of Starlink (left) and RSONAR (right)

The pixels generated from the Canny filter need to be grouped and labeled as unique objects. The Python library, *skimage*, was particularly useful for performing this task [43]. Initial steps included filling small discontinuities in the detected objects, while removing stars and random high frequency noise using *morphology* functions from the *skimage* library [43]. The size threshold for filtering out objects varied for each dataset, given that streaks and stars differed in size due to factors such as resolution, observer's focal length and zoom. Other variables which influenced the size threshold were the exposure times and the quantity of stacked images. Longer exposure times and a larger number of stacked images can produce streaking stars in the background which require consideration when establishing the size threshold. After filtering smaller objects, only the presence of an RSO or obstruction will remain in the final output image, as depicted in Figure 4.5. Conversely, if no RSO streak or obstruction is detected, the output image will be empty.

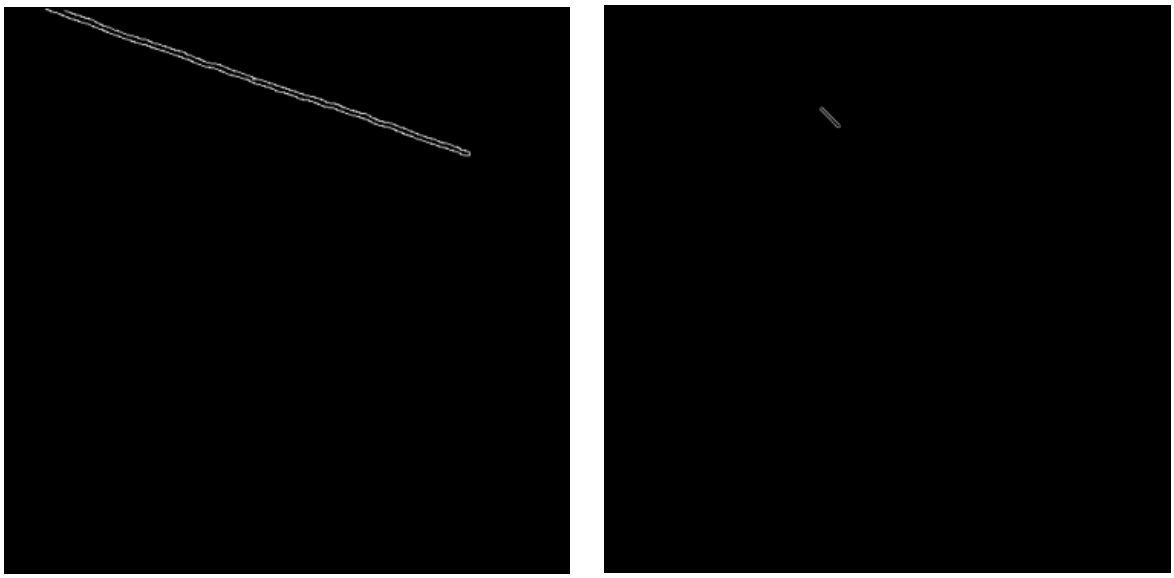

Figure 4.5: Starlink Observation (left) and RSONAR Images (right) with Small Objects Removed

The *measure* function from the *skimage* library was used to label the remaining objects using an 8-connectivity approach, which scans for neighboring connections vertically, horizontally, and diagonally to group them together [43]. This function also produces details regarding each labeled object, including its area and semi-major axis lengths. Subsequently, the final image and the data related to the labeled objects are cross-referenced with the sorting criteria to determine the appropriate folder for the image sequence.

4.2.3: Sorting Criteria

The sorting of these image sequences involves the creation of a .txt file named after the first image in the sequence, containing all the image names in the sequence. Text files are created instead of physically relocating or duplicating image sequences into the folders for several reasons. Primarily, the objective was to classify image sequences without disrupting the original databases. Dividing a night's observation into various folders disrupts the time of the database which may affect future analysis. While the images could be copied into a designated folder, this would require additional storage space and might be impractical for large datasets. If necessary, a straightforward script can be written to read the text file and duplicate some, if not all, sequences. In Folder 1, the text files containing potential RSO streaks are created, while Folder 2 contains text files solely of sequences with no objects other than stars and noise. Lastly, Folder 3 is reserved for images with potential issues like obstructions.

At this stage in the image processing pipeline, both stars and random small, high frequency noise have been removed. The classification tool then checks for the presence of objects in the output image. If no objects are found, indicating that the image sequence solely contains stars, the sequence is classified into Folder 2. If the output image is not empty, the algorithms distinguishes whether the object(s) present are potential RSOs or an obstruction. This

decision is made by assessing the persistence of detected objects throughout the image sequence. The image sequence is split into two halves, and the average lengths of the objects in each half are summed. These sums are then compared against the average object lengths in the complete stacked image sequence. Equation 4.1 summarizes this comparison, presenting a ratio where L_1 and L_2 represent the average lengths of objects in the first and second halves of the sequence. L_T stands for the average lengths in the complete stacked image sequence. After studying various obstruction versus RSO scenarios, a threshold of 1.3 was set to accommodate error margins caused by noise and errors.

$$ratio = \frac{\sum L_1 + \Sigma L_2}{\sum L_T} \quad 4.1$$

If the calculated ratio is below this threshold, the detected object is likely an RSO, and the sequence will be sorted into Folder 1. Conversely, if the ratio is equals or exceeds the set ratio, the object is deemed likely an obstruction, and the sequence belongs in Folder 3. In summary, the methodology developed a comprehensive image classification pipeline, focusing on object detection and categorization, allowing for the sorting of image sequences through bulk processing.

4.3: Testing

4.3.1: Data Preparation and Labelling

To assess the accuracy of the classification tool, the truth data needed to be acquired from each dataset. Acquiring truth data entailed manual inspection of each dataset to determine which images contained RSOs, empty star fields, or obstructions. Since no single dataset contained all three scenarios, diverse datasets were utilized to test obstruction and RSO streak detection. The CASSIOPE FAI dataset primarily facilitated the development of obstruction detection. Given the

classification tool's primary objective of detecting RSO streaks, the focus predominantly revolved around refining this aspect of the tool. Smaller datasets like Starlink Observations and the Torrance 2021 Field Campaign were comparatively simpler to label due to distinct streaks were, smaller databases, and manageable manual sorting times.

Meanwhile, datasets such as RSONAR and NEOSSat were significantly larger with thousands of images available. To mitigate this challenge a subset from each data set was chosen for testing. In RSONAR, a random subset of 2,700 images between the periods of ascension and descension of the mission was chosen. To expedite the manual labeling process, sequences of 27 images were stacked for visual inspection, facilitating the labeling of potential RSO streaks. For NEOSSat images, tracks containing streaks were sought out from the online database, and a subset of 82 images was selected for testing streak detection. Despite efforts to ensure precise labeling, it's essential to acknowledge the presence of limitations and potential human errors when manually labeling a dataset.

4.3.2: Procedure

Once truth data is obtained for each dataset, the classification tool processes the labeled data. Each output from the classification tool is then cross-referenced with the manually labeled data to determine its accuracy. The accuracy was quantified by calculating the sensitivity and specificity of the algorithm using the following calculations [44]:

$$Sensitivity = \frac{TP}{TP+FN} \quad 4.2$$

$$Specificity = \frac{TN}{TN+FP} \quad 4.3$$

$$Accuracy = \frac{TN+TP}{TN+TP+FN+FP} \quad 4.4$$

These equations use the measurements of True Positives (TP), True Negative (TN), False Positive (FP), and False Negative (FN) [44]. This quantitative method of determining accuracy offers a comprehensive view of the classification tool's limitations and successes by highlighting sensitivity and specificity. The results for RSO streak detection, using these parameters, are summarized in Table 4.1. However, due to the classification tool's focus on RSO streak detection and the limited obstruction data, the testing on the obstruction capability wasn't quantifiably performed.

4.4: Results

Table 4.1: Summary of Results from RSO Streak Detection Testing

	TP	FP	TN	FN	Sensitivity (%)	Specificity (%)	Accuracy (%)
Torrance 2021 Campaign	15	0	901	0	100	100	100
NEOSSat	6	14	60	2	75	81	80.49
RSONAR (Stacks of 27)	4	10	86	0	100	89	90
RSONAR (Stacks of 9)	4	4	292	0	100	98.6	98.67

Results were not calculated for the Starlink Observation images as they were primarily utilized in developing the algorithm. The classification tool worked well with the Torrance 2021 Field Campaign images due to the clear visibility of streaks and manageable noise levels. This ground-based observer had an exposure time ranging from 3 to 5 seconds, enabling the capture of longer streaks and filling the sensor with more information compared to shorter exposure

times. The higher resolution of the field campaign images, set at 2048 x 2032, contributed to easier streak detection despite causing processing delays. A demonstration of a streak from a single Torrance 2021 Field Campaign image is depicted in Figure 4.6 to show their clarity.

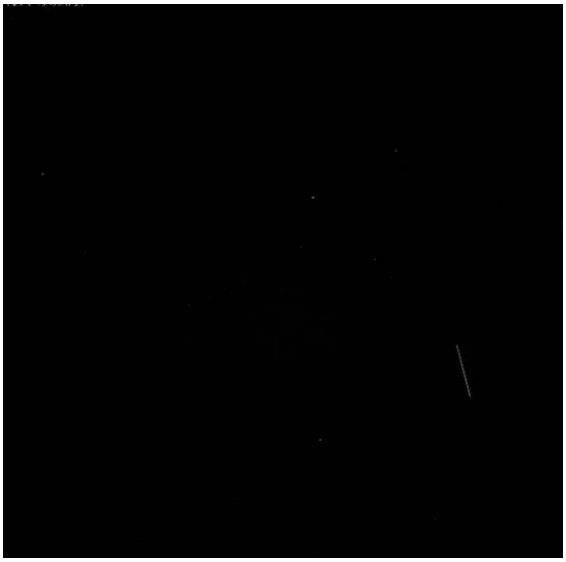

Figure 4.6: Torrance 2021 Field Campaign Streak

NEOSSat images posed a unique challenge that significantly impacted the accuracy of the classification tool. In some scenarios, stars oversaturated pixels and spilt over, creating a streak-like shape shown in Figure 10. These star streaks often resulted in false positive results, misleading the classification tool into interpreting them as streaking RSOs. This highlighted a lack of specificity in the tool's detection mechanism. However, oversaturated stars that were small as seen in Figure 10, were still filtered out as they fell below the size threshold set for star filtration. Furthermore, NEOSSat images contained troublesome high-frequency noise that proved challenging to manage without excessively smoothing the image. Over-smoothing led to false negatives, causing very dim objects to be overlooked during detection as their intensities blended into the background. As mentioned previously, individual processing of these images due to varying resolutions significantly extended computation times.

Finally, the RSONAR images were tested using two different image stack sizes. Stacks of 9 performed better, effectively retaining dimmer objects during stacking, and achieving a more balanced noise reduction. Conversely, the stacks of 27 presented challenges, resulting in a higher number of false positives. Sway and instability from the high-altitude balloon payload caused stars to cluster in sizes that exceeded the set size threshold. Additionally, to prevent dim objects from being further dimmed during stacking, a less aggressive noise reduction approach was applied. Unfortunately, this approach left behind large high-frequency noise, which was then picked up by the Canny Filter. Despite these drawbacks, larger stacks were necessary for detecting images where RSOs were point sources and stacked to form streaks. Although the subset of 2,700 images didn't contain that specific scenario, the stack size was tested on a smaller subset of 61 images, successfully detecting the stacked streak. Depending on the image sequence's starting point, stacking 9 images sometimes missed the stacked streak. However, in the test on the 2,700-image subset, the stack of 9 images outperformed the 27 image stacks in specificity and accuracy. In both scenarios, no detections were missed, as the tool prioritized sensitivity over specificity.

To enhance the specificity of this algorithm, future approaches that focus on the shape of the detected object could be valuable. While good accuracies were achieved in some datasets, one of the drawbacks of this algorithm is the computation power and time required. Despite attempts to address this issue through stacking and bulk processing, there is room for improvement. Both the Wiener and Canny filters use a significant number of resources, contributing to more complex and slower processes. Hence, the classification tool is currently more suitable as a post-mission tool rather than a real-time onboard algorithm.

Chapter 5: Initial Orbit Determination

5.1: Overview

The implementation of an IOD method on a space-based observer, CASSIOPE's FAI, stands as a fundamental stride within a broader endeavor toward refining resident space object (RSO) identification. RSO identification entails correlating observed paths of unknown objects with the TLE propagated paths of catalogued objects. Through RSO identification, observed objects can be characterized and explored to deepen understanding of their orbital behavior. The introduction of IOD is a fundamental milestone which represents the initial phase of a larger orbit determination framework, aiming to enhance RSO identification by integrating more points of comparison. Figure 5.1 illustrates the IOD's role in this overreaching objective and framework.

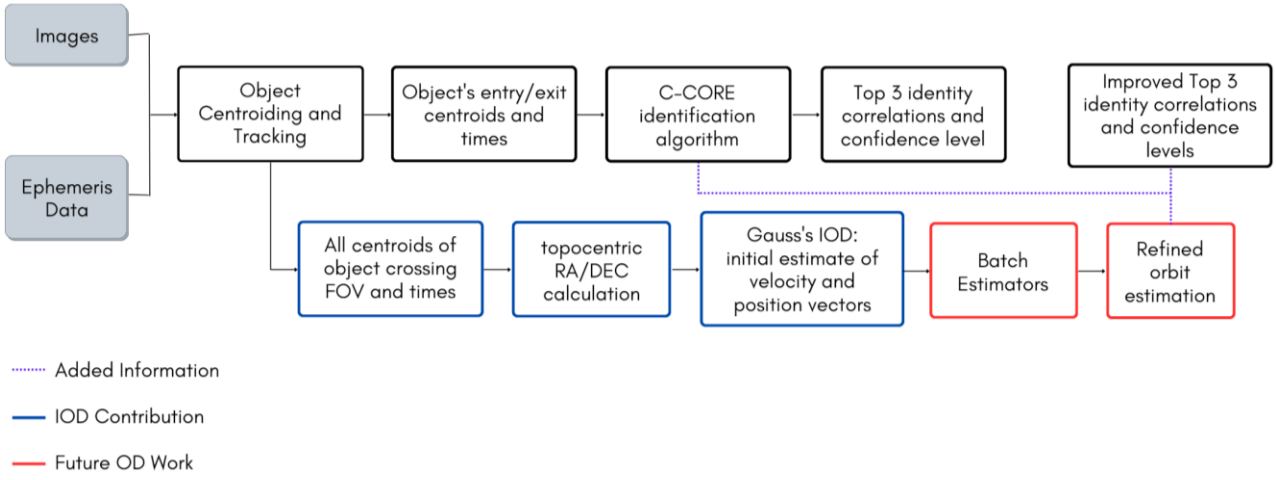

Figure 5.1: Identification Framework with Proposed Improvement Pipeline

The chosen initial orbit determination method, Gauss's method, serves as an initial step in a long and complex process of augmenting the existing identification pipeline using orbit determination. Gauss's IOD serves to provide an initial estimate of the orbital parameters of an

object observed via a space-based optical sensor. The use of an optical sensor adds a layer of complexity to the implementation of an IOD method to this framework as other observation sensors such as radio frequency (RF) can provide more accurate angular measurements. The primary objective of this work was to bridge the gap between space-based optical observations and a classical IOD method, thereby providing an initial estimate of orbital parameters. A large focus of the work was on establishing the connection between optical measurements and the input requirements of Gauss's IOD method. The approach of using IOD as a preliminary step, followed by an optimizing OD phase, is a method frequently referenced in research [7][45][46]. Research has demonstrated that an IOD initial guess provided better convergence times than random initialization values [47]. Batch estimators, like least squares or Kalman filters, are used to minimize residuals and provide more precise estimations of orbital parameters [45]. The preliminary estimate will undergo further refinement using a batch optimizer and will ultimately be reintegrated into the existing RSO identification framework by other members of the Nanosatellite Lab at York University. This proposed improvement aims to provide further points of comparison for correlating the orbit with a catalogue ID.

A review of classical IOD methods was conducted to find the most suitable approach for this specific application. Given the available information from optical images, angles-only methods were considered. Gauss's method was chosen as the preferred choice, partly due to its effectiveness in handling smaller spreads of data, ideally those separated by 10 degrees or less [11]. The observation data available consists of a single pass of an RSO on an optical sensor with a field of view of 26 degrees. These conditions result in observation points that are close together. In contrast, other IOD methods typically perform better with observation points that are further apart from each other. Gauss's IOD method also benefits from iterative improvement,

refining the accuracy of state vector calculations. Overall, Gauss's method demonstrates moderate robustness and works well with low-Earth objects.

5.2: Existing Identification Method

Understanding how the current identification algorithm (originally developed by C-Core) works is the first step in determining ways in which the algorithm can be augmented. This existing algorithm integrates TLE data, ephemeris information, optical sensor data, and centroid information of the observed object as it enters and exits the observer's field of view. The TLE information is obtained from Spacetrack.com for the specific day of observation [13]. The centroid information is extracted using automated centroiding algorithms for greater accuracy. Utilizing the previously described neural network approach, RSOnet, assists in centroid information extraction [9]. The identity correlation algorithm generates the three best potential matches for the detected object's identity, along with a confidence rating based on the ratio between the top two matches. Figure 5.2 provides an example of an object which was labelled using the top identity match.

Figure 5.2: Object Labeled in Real FAI Image Using Identity Correlation Algorithm

This algorithm initiates by propagating the orbits of both the observer and target objects using TLE data. The state vectors of the observer are calculated at the times when the object of interest enters and exits the observer's FOV. Following this, coordinate system conversions for each target object are performed and orthographic projection is applied to determine if and where the target object lies within the imager's field of view. During this first stage, the identification algorithm estimated the pixel locations that the RSO would have appeared in the observer's FOV based on TLE and sensor information. Subsequently, the calculated target locations are compared to the pixel locations where the target was observed in the images. The comparison focuses on three main areas: the entry point, the exit point, and the assumed path between these two points. The assumed path of the object is estimated by drawing a straight line between entry and exit points.

A cost function is employed to quantify the comparison of these distinct points. The catalogue object with propagated points that are closest to the observed points of the object in the image will have the lowest cost function value. The catalogue object's propagation which yields the lowest cost function value is considered the top identity result. Additionally, the algorithm provides a confidence level value, indicating its confidence in the top result. The confidence level is calculated by comparing the cost value of the second result with that of the first one. If the confidence level of the identity correlation is above a threshold of 4, then it is considered an accurate identity label. Figure 5.3 outlines the inputs, outputs, and flow of the identity correlation process.

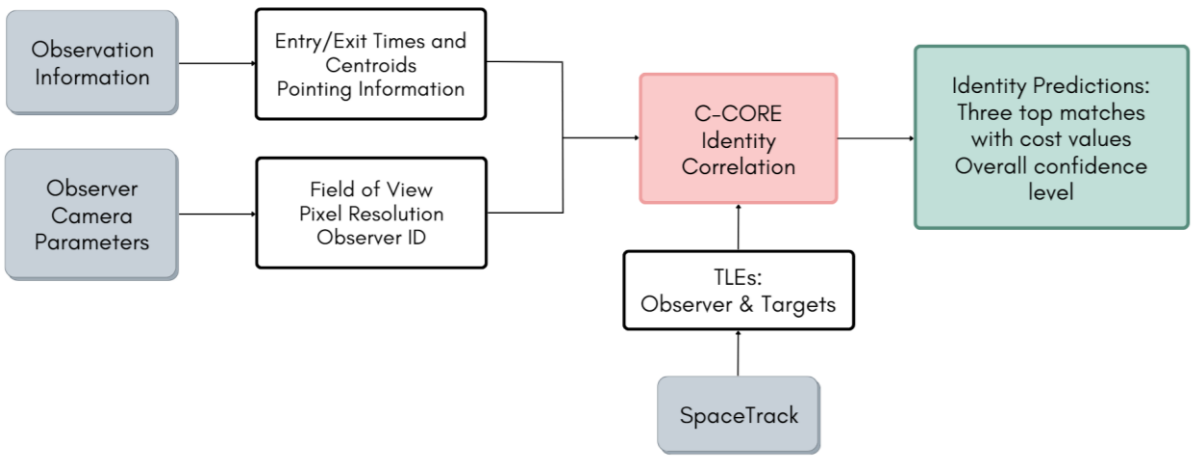

Figure 5.3: Overview of identification algorithm inputs and outputs

The goal of introducing IOD is to incorporate additional points of comparison beyond the three points of comparison currently used in the identification algorithm. Instead of solely considering the object's path from its entry and exit points, the proposed method looks at the entire path of the observed and propagated objects. This approach allows the identification algorithm to evaluate a greater set of points when determining the cost function value and performing its identity correlation.

5.3: Space Application of Gauss's Initial Orbit Determination

5.3.1: Input Data from Simulated Images

For the application of Gauss's Initial Orbit Determination on data collected from Cassiope's FAI imager, the simulator SBOIS was used. The SBOIS generated images, as shown in Figure 5.4, contained information on ephemeris data and the identity of the RSO within the simulated image.

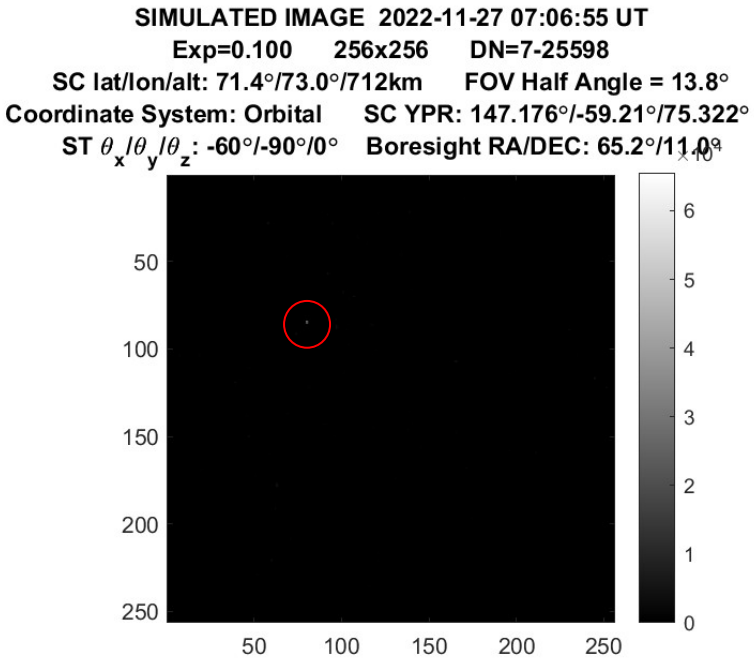

Figure 5.4: Simulated image used for IOD with RSO labeled in red circle.

The simulated data facilitated both the development and verification of a Gauss's IOD method application on a space-based observer. To implement Gauss's IOD algorithm the following inputs are required:

- Three observation times
- Topocentric RA and DEC to the satellite from the observer at each observation
- Position vectors of the observer at each observation time

Three distinct observation times are selected during the transit of an object of interest across the observer's FOV, emphasizing separation between these observations. The selection of observation points differs from the identification algorithm, which uses the moments of the RSO entering and exiting the observer's FOV. The selected observation times are all different from

those used in the identification process. While the three observations times can be directly extracted from the simulated image data, the topocentric RA and DEC and position vectors of the observer need to be calculated.

The pixel locations of the RSO at each observation and the central RA and DEC values were directly extracted from the simulated image data. This information is used to calculate the topocentric RA/DEC from the observer to the target RSO using an inverse spherical orthographic projection approach. First, the observer's conic half angle in both x and y directions, representing the FOV of the imaging system is calculated. Subsequently, the conic half angles are used in a rectilinear grid approach to convert the pixel locations into projections on the orthographic planes using the following equations [36].

$$X = \left(x_p - \frac{s_x}{2}\right)\left(\frac{sin(FOV_x)}{\frac{s_x}{2}}\right) \quad 5.1$$

$$Y = \left(y_p - \frac{s_y}{2}\right)\left(\frac{sin(FOV_y)}{\frac{s_y}{2}}\right) \quad 5.2$$

This method is followed by spherical coordinate calculations, involving trigonometric functions, to estimate the topocentric RA and DEC of the RSO relative to the observer's position. These calculations involve the following equations, where p represents the radial distance from the observer to the RSO and c denotes an angle that signifies the angular position in relation to the radial distance:

$$p = \sqrt{x^2 + y^2} \quad 5.3$$

$$c = arcsin(p) \quad 5.4$$

Finally, the spherical calculations are concluded with the calculation of the topocentric RA and DEC values using the following equations:

$$DEC = arcsin\left(cos(c) \cdot sin(DEC_0) + \frac{Y \cdot sin(c) \cdot cos(DEC_0)}{p}\right) \quad 5.5$$

$$RA = RA_0 + arctan\left(\frac{X \cdot sin(c)}{p \cdot cos(c) \cdot cos(DEC_0) - Y \cdot sin(c) \cdot sin(DEC_0)}\right) \quad 5.6$$

Note that RA and DEC represent the topocentric values while RA_0 and DEC_0 represent the central boresight values provided in the simulated data. The methodology of the topocentric RA/DEC calculations was an inversion and adaptation of a function in the SBOIS simulator which estimated the pixel location of an RSO in the observer's FOV [36]. Following these calculations, the remaining inputs to be calculated are the position vectors of the observer at each observation time. The times and observer's ID are first extracted for the simulated images. Subsequently, using the observer's TLE obtained from Spacetrack.org, the observer's location is backwards propagated to the observation times. This propagation is carried out using the *sgp4.api* tool in Python, which returns the observer's cartesian position and velocity vectors [48]. The culmination of these calculations provides the essential groundwork and inputs for the chosen initial orbit determination method.

5.3.2: Gauss's Initial Orbit Determination: Preliminary Estimation

Gauss's Initial Orbit Determination uses at minimum three observations at different times to allow for an initial estimate of state vectors and orbital elements. This methodology uses mathematical computations to iteratively solve equations, allowing for a better estimation of an RSO's orbit. Gauss's method starts by using the topocentric RA and DEC values for calculating the line-of-sight vectors to the RSO as depicted by ρ in Figure 5.5 and L_i in equation 5.7

[49][11]. These line-of-sight vectors, also known as topocentric direction cosine vectors, are calculated using equation 5.7 where δ is the declination and α is the right ascension [11]:

$$\hat{L}_i = \begin{bmatrix} \cos(\delta_{ti})\cos(\alpha_{ti}) \\ \cos(\delta_{ti})\sin(\alpha_{ti}) \\ \sin(\delta_{ti}) \end{bmatrix} \quad i = 1\ldots3 \tag{5.7}$$

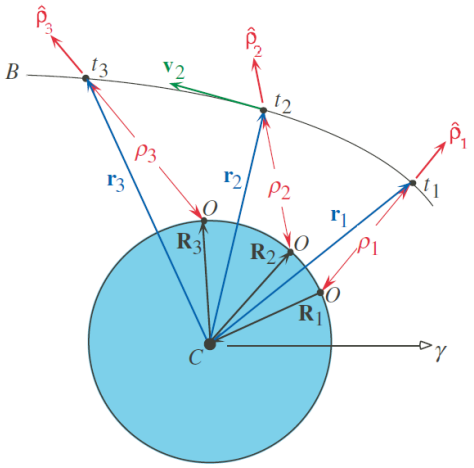

Figure 5.5: Illustration of Observations and Relevant Vectors Used in IOD

The time intervals, τ_1, τ_3, τ, were calculated using equation 5.8 and were centered around the middle observation, t_2:

$$\begin{aligned} \tau_1 &= t_1 - t_2 \\ \tau_3 &= t_3 - t_2 \\ \tau &= \tau_3 - \tau_1 \end{aligned} \tag{5.8}$$

The line-of-sight vectors were combined into three pair combinations and their cross products were calculated. The scalar triple product, D_0, and six scalar quantities were then calculated using the observer's position vectors and the cross products of the line-of-sight

vectors. These scalar quantities are used in subsequent calculations of other variables that are required for Newton's method as shown in equation 5.9:

$$x_{i+1} = x_i - \frac{x_i^8 + ax_i^b + bx_i^3 + c}{8x_i^7 + 6ax_i^5 + 3bx_i^2} \quad 5.9$$

Newton's method involves a higher order polynomial and therefore requires iterative processing to solve. This method starts by finding the roots of the polynomial in the numerator to locate the inflection point from negative to positive. This value is used as the starting point for solving equation 5.9. The value where x converges represents the geocentric radius, denoted as r_2. The geocentric radius, along with the scalar quantities, time intervals, and Earth's gravitational parameter, are then used to compute the slant ranges, ρ_1, ρ_2, ρ_3. These slant ranges are used in determining the geocentric position vectors, r_1, r_2, r_3, used for approximating the Lagrange coefficients. The estimation equations are derived under the assumption that τ_1 and τ_3 are small enough, so the first two terms of the series expressions are the only ones retained as seen in equations 5.10-5.13 [49].

$$f_1 \approx 1 - \frac{1}{2}\frac{\mu}{r_2^3}\tau_1^2 \quad 5.10$$

$$f_3 \approx 1 - \frac{1}{2}\frac{\mu}{r_2^3}\tau_3^2 \quad 5.11$$

$$g_1 \approx \tau_1 - \frac{1}{6}\frac{\mu}{r_2^3}\tau_1^3 \quad 5.12$$

$$g_3 \approx \tau_3 - \frac{1}{6}\frac{\mu}{r_2^3}\tau_3^3 \quad 5.13$$

Using these estimations of Lagrange coefficients and the geocentric position vectors from the first and third observations, the velocity vector at the second observation, v_2, is then approximated.

5.3.3: Iterative Improvement of Preliminary State Vector Calculations

The estimated state vectors, r_2 and v_2, undergo further refinement through an iterative process. The iterative improvement aims to take the approximations of Lagrange coefficients and refine them further to subsequently improve state vector estimations. This process begins by calculating the magnitude of the position vector, r_2, at t_2, and the velocity vector's magnitude, v_2, to compute the reciprocal of the semimajor axis and radial component. The universal Kepler's equation is applied to solve for the universal values χ_1, χ_3, at the first and second observation times:

$$\sqrt{\mu}\tau_1 = \frac{r_2 v_{r2}}{\sqrt{\mu}}\chi_1^2 C(\alpha\chi_1^2) + (1-\alpha r_2)\chi_1^3 S(\alpha\chi_1^2) + r_2\chi_1 \quad 5.14$$

$$\sqrt{\mu}\tau_3 = \frac{r_2 v_{r2}}{\sqrt{\mu}}\chi_3^2 C(\alpha\chi_3^2) + (1-\alpha r_2)\chi_3^3 S(\alpha\chi_3^2) + r_2\chi_3 \quad 5.15$$

The universal values are used to calculate updated Lagrange coefficients. The updated values are used to determine the coefficients, c_1 and c_3:

$$c_1 = \frac{g_3}{f_1 g_3 - f_3 g_1} \quad 5.16$$

$$c_3 = -\frac{g_1}{f_1 g_3 - f_3 g_1} \quad 5.17$$

Following the coefficient calculation, these values are used to calculate three revised slant range values and subsequently, updated position vectors, r_1, r_2, r_3, and the velocity vector, v_2. This series of calculations, from determining the magnitude of a preliminary r_2 and v_2 to

updating those same values following the updates of Lagrange Coefficients, are repeated until the values of the slant ranges stop changing or meet the desired precision. After completing Gauss's IOD and the iterative improvement process outlined in Figure 24, the state vectors are converted to orbital parameters.

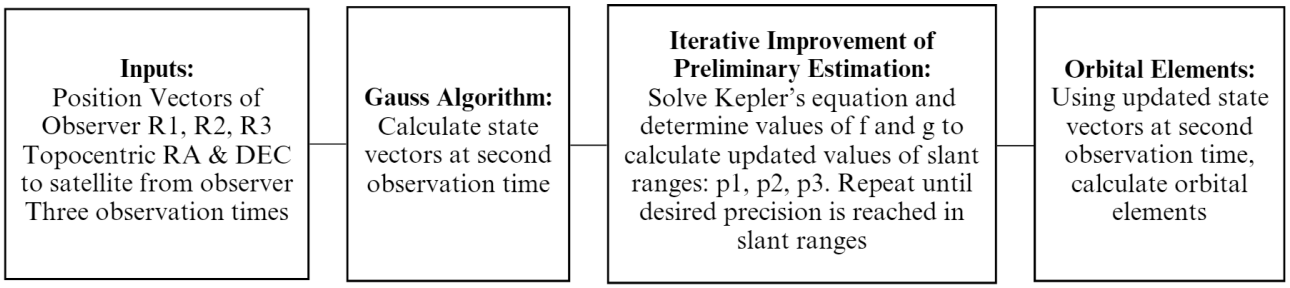

Figure 5.6: Summary of Gauss's IOD Algorithm

5.3.4: Limitations of Gauss's Initial Orbit Determination

IOD methods such as Gauss's method often act as an initial step for orbit determination rather than a standalone approach due to their limited accuracy. Gauss's IOD is particularly sensitive to measurement errors, and in this specific application, multiple sources of errors lead to limitations in the accuracy of the IOD output. The centroid calculations for objects within the optical image pose the initial source of uncertainties. Achieving perfect sub-pixel accuracy in centroid calculations can be challenging. The main source of limitations may arise from the topocentric RA and DEC calculations. These calculations involve using estimated centroid pixel locations, central RA and DEC boresight measurements, and sensor variables, aiming to estimate a vector from the observer to the unknown object. The accuracy of this method is limited as it is difficult to estimate the topocentric vector without knowing the state vectors of the unknown object. Instead, the only available information is the pixel positions on a 2D image generated on the observer's sensor.

Another contributing factor to measurement error comes from estimating the observer's state vectors using TLEs. TLE propagation, despite being a common method, entails small errors that could introduce uncertainties into the IOD process. Furthermore, limitations could also arise due to the brief observation arc in this scenario. While Gauss's method is most effective with observations featuring short separations, in this scenario, the separations were as brief as 25 seconds apart, significantly restricting the available information for determining the state vectors of the unknown object [11]. Additionally, Gauss's method doesn't account for non-gravitational influences such as solar pressure, which could result in discrepancies during orbit parameter calculations.

5.3.5: Results

The state vectors estimated by Gauss's IOD method are converted to six orbital parameters: Eccentricity (e), Right Ascension of Ascending Node (RAAN) (Ω), Inclination (i), Argument of Perigee (ω), True Anomaly (θ), and Semi-Major Axis (a). Orbital elements are parameters used to define a spacecraft's position in both space and time. These elements encompass details about the orbital plane, the object's location within that plane, and the orientation of the orbit in three dimensions [49]. Figure 5.7 provides a visual representation of the aspects of the orbit which the orbital elements describe [49]. It's worth noting that while the diagram lacks the representation of the Semi-Major Axis, this element specifies the longest diameter of an ellipse. Estimation of the orbital parameters allowed for a more visual comparison and understanding of discrepancies in results. Additionally, the Python library, *ORBDTOOLS,* produced results in the form of orbital elements, necessitating the conversion from state vectors to orbital elements for the comparison of IOD methods [50].

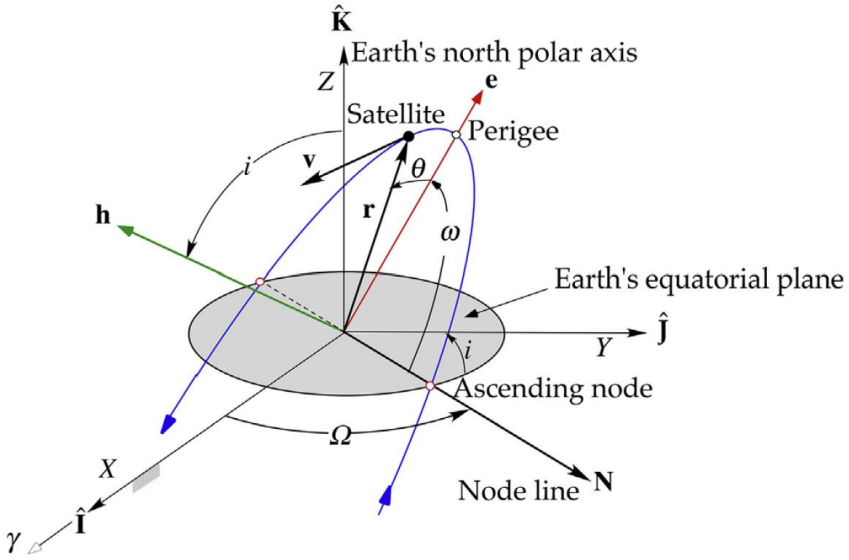

Figure 5.7: Visualization of Orbital Elements

Although the state vectors of the target RSO will be used in the subsequent optimization steps, they were converted to orbital parameters to evaluate the result accuracy. Comparison of the outputs derived from the implemented Gauss's IOD algorithm was conducted against results obtained from other classical IOD methods sourced from available Python libraries [50]. Table 5.1 presents the results of other IOD methods from the same set of optical observations. Exploring which orbital elements had larger discrepancies illustrated the magnitude of errors for each IOD method. The TLE data of the target RSO was used to compute the same six parameters to compare the accuracy of each method. The significant digits accuracy of these results was set to the lowest accuracy present in the TLE of the target object.

While certain parameters from other IOD methods better matched the values from the TLE, Gauss's method displayed overall smaller deviations compared to the other classical methods. The eccentricity and semi-major axis elements describe the shape and size of the orbital plane [11]. Gauss's method, having the lowest discrepancies for both eccentricity and

semi-major axis, thus offered a representation of the orbital plane's shape and size that was closest to the truth data. While some methods, such as Laplace, shared the same eccentricity estimation value, their semi-major axis estimation had significant errors. However, Gauss's method, despite having smaller errors for eccentricity and semi-major axis, still failed to provide precise estimations for other methods such as the RAAN, Argument of Perigee, and True Anomaly. Consequently, it failed to provide an accurate description of the orbital plane's orientation and object's location within that orbit.

Table 5.1: Comparison of Orbital Parameter Estimations from Different IOD Methods

	From TLE (Truth Data)	Gauss	Laplace	Goodings	Double-R
Eccentricity	0.0021	0.0601	0.0601	0.9999	9.1243
RAAN (deg)	335.7690	93.9172	93.9174	321.0640	218.3140
Inclination (deg)	98.1995	81.0818	81.0818	96.4613	65.3424
Argument of Perigee (deg)	312.9210	194.8040	195.0330	68.7364	70.4015
True Anomaly (deg)	136.2970	-83.1714	270.3160	358.5330	22.9358
Semi-Major Axis (km)	7076.0300	7116.2300	1.1154	22842.3000	-0.1356

The observed discrepancies among the IOD methods highlight the challenges in accurately determining orbital parameters solely from a single pass of space-based optical observations. These inaccuracies emphasize the need for further refinement of the results from IOD methods for enhanced accuracy. IOD serves as a preliminary step within a broader orbit determination process where the state vectors undergo refinement. Starting from an initial estimation of state vectors can facilitate better convergence during the optimization stage in OD, thereby establishing IOD as a crucial initial step [7][45][46].

Chapter 6: Conclusion and Future Work

6.1: Overview of Thesis

Continued contributions to SSA research remain pivotal in enhancing efforts in mitigating congestions within Earth's orbits. Our reliance on current space technology, such as GPS and satellite internet makes SSA strategies crucial. Given the increasing use of ground and space-based sensors, research into harnessing the capabilities of these datasets becomes a critical aspect of SSA. These optical sensors, spanning from repurposed star trackers to innovative technologies tailored explicitly for SSA research, offer diverse datasets, each presenting unique challenges. Diverse datasets offer a great range of different challenges which therefore require flexible and robust algorithms that can adapt to each dataset. Protecting Earth's orbits from additional debris generated from inadvertent collisions remains key to sustaining the safety and functionality of present and future space assets.

This thesis utilized six distinct databases, each with their own specific role in this work as discussed in Chapter 3. Studying these databases aimed to gain a deep understanding of their advantages and ideal use cases. The images studied came from ground, space, and near-space environments and used different hardware, offering wide diversity between datasets. Parameters such as resolution, labeled information, and exposure times were used to determine the ideal use case for each dataset. This profound comprehension further enhanced result interpretations, offering insights into the performance of tools like the classification tool and revealing both their strengths and weaknesses. Additionally, this knowledge guided the selection of datasets for testing the IOD implementation.

The initial effort towards contributing to SSA research in this thesis was an introduction to a classification tool designed to address challenges associated with large optical databases. As discussed in Chapter 4, the tool aimed to streamline the search for images containing RSO streaks, thereby reducing time and efforts typically spent in manual labelling. Some of the databases in which the classification tool was applied had thousands of images and would have taken significant times to manually label and search for streaks. By leveraging various image processing techniques, the classification tool effectively sorted images from a variety of databases. However, the variability among such as different sensors, environments, and capture parameters was challenging to deal with. This variability was good for testing the robustness of the classification tool. Despite the challenges faced, the tool demonstrated moderate robustness, excelling notably with the Torrance 2021 Field Campaign images when labelling images with RSO streaks.

Another objective of this thesis towards contributing to SSA research involved augmenting an existing identification algorithm by introducing Gauss's IOD algorithm. Accurate RSO identification is an important aspect of SSA as it allows for studying and tracking RSOs. The introduction of an orbit determination framework aims to augment the accuracy by adding information of the entire path of the object across the observer's FOV. The first step of an orbit determination framework is an IOD method to provide an initial guess for the batch optimizers. Following literature reviews, Gauss's method was determined as the most appropriate method for the data used in this work. The implementation on a space environment involved bridging the gap between the simulated images and Gauss's IOD method such as the calculation of topocentric RA/DEC. Gauss's IOD method was implemented on the space-based simulated FAI image data and an initial guess of the state vectors was determined. Following the state vector

calculations, the results were compared with those obtained using other IOD methods to assess the accuracies and limitations of different classical IOD methods.

6.2: Research Objectives and Contributions

The contribution of this work starts with the development of an image classification tool, specifically developed for sorting through images captured during campaigns conducted in the Nanosatellite Lab at York University. The image classification algorithm served as a post-processing tool for the RSONAR mission, effectively sorting through over 93,000 captured images [31]. Its primary focus was to determine which image sequences contained potential RSO streaks and which sequences only contained stars [31]. Through its use on large datasets, the objective of the classification tool was achieved by reducing the amount of time needed to manually sort through image sequences and find those containing RSO streaks.

In the course of this work, an existing RSO identification algorithm was studied, and its potential limitations were identified. Given the critical role of RSO identification in tracking and managing space objects and debris, enhancing the accuracy of this algorithm becomes imperative. Consequently, ways to improve the algorithm were explored, and the idea of adding new points of comparison by studying the entire path of the object through the image sequence was introduced. Following a literature review, orbit determination was proposed as an effective method for introducing these additional points of comparison. The work for this OD branch started with the implementation of an IOD method to provide an initial guess of the object's state vectors. After extensive research, Gauss's IOD method was chosen as a suitable angles-only candidate for this initial estimation. Despite encountering numerous challenges and limitations in adapting Gauss's IOD method to a space-based scenario, its implementation proved valuable.

Serving as the starting point for batch optimizers in the ongoing OD method implementation, it laid the foundation for subsequent analysis.

6.3: Future Work

Research on innovative techniques for SSA is an ongoing endeavor, especially within the Nanosatellite Lab. The findings of this research serve an important role in aiding the advancement of other ongoing and future projects. The classification tool developed can be used on current campaign databases and future RSONAR missions, facilitating image sorting and allowing for performance comparisons with alternative object detection methods. Meanwhile, the implemented IOD methodology is currently being used by other peers as the initial step for an OD method aimed at improving the existing identification algorithm. The examination of limitations conducted in this research not only provides insights into the inherent constraints of Gauss's method for the specific scenarios used in this work but also aspires to contribute ideas for enhancing accuracy. The goal of the work developed throughout this research is to provide new insights and foundational steps to foster the development of new strategies for SSA efforts.

6.3.1: Image Classification Future Work

The image classification tool demonstrated varying performance across databases, excelling with some while struggling with others, such as NEOSSat. Test results highlighted a need for improvements in a few areas. One potential enhancement involves incorporating shape analysis to differentiate between objects of interest, artifacts, and noise. Current thresholding parameters, primarily reliant on size, occasionally presented limitations, as observed in NEOSSat images. These limitations were evident in images where saturated pixels from bright stars appeared as streak-like objects. Upon closer inspection, these artifacts displayed a unique wider

center compared to the ends, distinguishing them from RSO streaks that tend to have uniform widths. Additionally, high-frequency noise sometimes created large objects above the size threshold, resulting in false positives. Shape analysis holds promise in differentiating between artifacts, noise, and streaks by discerning subtle differences in shapes.

The classification tool was used on different databases with varying environments, hardware, and capture parameters. The calibration of parameters such as stacking sizes, filter sizes, and thresholds for different databases can be time-consuming. Streamlining the calibration of parameters for different databases by increasing the tool's modularity could reduce pre-scanning efforts. Moreover, optimizing the processing times of complex techniques such as the Weiner and Canny filters is essential for more efficient processing. While bulk processing alleviates some processing times, further optimizations can enhance the tool's efficiency.

Expanding the scope of SSA research, integrating the classification tool with existing identification methods could create a comprehensive pipeline for detecting, extracting, and identifying streaks. This integration would bridge gaps between algorithms, by introducing a streak extraction method to cleanly extract information about the detected streak such as endpoints. The extracted information would be used for adding streak identification to the existing identification method. Such advancements would allow focus on studying the detected objects and their trajectories, enhancing our understanding of them.

6.3.2: Initial Orbit Determination and Identification Future Work

As outlined in Chapter 5 and illustrated in Figure 20, Gauss's IOD method served as a preliminary step in a greater framework for RSO identification. The subsequent work aims to refine state vectors estimated from Gauss's IOD using a batch optimizer. Evaluating various

batch estimators like least squares Powell's dogleg, or Kalman filtering and determining the optimal number of observations will be important steps [7]. Once the OD portion of the framework is finalized and results have been refined to an acceptable accuracy, the next goal will be to integrate these points of comparison back into the existing identification method.

One potential integration method involves modifying the cost function to incorporate results from OD. Currently, the cost function uses weighted addition of current comparison points to determine a cost value. All the identity options are sorted based on their cost function values to determine which is the best option. Adding a weighted point based on the results of OD could be a useful way to seamlessly integrate OD results back to the identification algorithm. This point could compare the state vectors from OD to those from each TLE of all target options. The integration could improve the identity correlation accuracy, impacting efforts of RSO tracking and analysis of objects for SSA.

References

[1] *Advancing Space Situational Awareness for National Security*. HDIAC. (2021, May 14). https://hdiac.org/articles/advancing-space-situational-awareness-for-national-security/

[2] Canadian Space Agency. (2018, February 8). *10 ways that satellites helped you today*. https://www.asc-csa.gc.ca/eng/satellites/everyday-lives/10-ways-that-satellites-helped.asp

[3] Iyer, S. (n.d.). *Data Sources*. Retrieved May 18, 2022, from http://astria.tacc.utexas.edu/AstriaGraph/

[4] Oltrogge, D., & Kelso, T. S. (2011, August 01). Getting to know our space population from the public catalog.

[5] *Space situational awareness – A quick overview*. New Space Economy. (2023, April 25). https://newspaceeconomy.ca/2022/11/22/space-situational-awareness-a-quick-overview/

[6] Weeden, B. (2017, May). Space situational awareness fact sheet. https://swfound.org/media/205874/swf_ssa_fact_sheet.pdf

[7] Sciré, G., Santoni, F., & Piergentili, F. (2015). Analysis of Orbit Determination for space based Optical Space Surveillance System. *Advances in Space Research, 56*(3), 421–428. https://doi.org/10.1016/j.asr.2015.02.031

[8] Yekkehkhany, B., Shokri, P., & Zadeh, A. (2020). A computer vision approach for detection of asteroids/comets in space satellite images. *The International Archives of the Photogrammetry, Remote Sensing and Spatial Information Sciences, XLIII-B3-2020,* 1185–1190. https://doi.org/10.5194/isprs-archives-xliii-b3-2020-1185-2020

[9] Dave, S., Clark, R., & Lee, R. S. (2022). RSOnet: An image-processing framework for a dual-purpose star tracker as an opportunistic space surveillance sensor. *Sensors, 22*(15), 5688. https://doi.org/10.3390/s22155688

[10] Lovell, T. A., Sinclair, A. J., & Newman, B. (2018). Angles only initial orbit determination: Comparison of relative dynamics and inertial dynamics approaches with error analysis. *2018 Space Flight Mechanics Meeting*. https://doi.org/10.2514/6.2018-0475

[11] Vallado, D. A. (2013). Fundamentals of Astrodynamics and Applications (4th ed.). Microcosm Press.

[12] Dolado, J., Yanez, C., & Anton, A. (2016). On the performance analysis of Initial Orbit Determination algorithms.

[13] Space-Track.org. (n.d.). Frequently Asked Questions. Space-Track.org. https://www.space-track.org/documentation#/faq

[14] Kelso, T. S. (2023, October 23). *"Frequently Asked Questions: Two-Line Element Set Format"* CelesTrak. https://celestrak.org/columns/v04n03/#FAQ01

[15] Picot, J. (2020, August 23). *Where and how to get the orbital parameters (two-line element) of a satellite over a period of time? NORAD Tutorial*. Medium. https://josephinepicot.medium.com/where-and-how-to-get-the-orbital-parameters-two-line-element-of-a-satellite-over-a-period-of-time-f955f65b6cb

[16] Pastor-Rodríguez, A., Escobar, D., Águeda, A., & Sanjurjo-Rivo, M. (n.d.). Correlation techniques to build-up and maintain space objects catalogues. Madrid, Spain. Retrieved from https://indico.esa.int/event/224/papers/3861/files/217-Correlation_techniques_to_build-up_and_maintain_space_objects_catalogues.pdf

[17] Ackermann, Mark R., Cox, David D., Kiziah, Rex R., Zimmer, Peter C., McGraw, John T., & Cox, David D. *A systematic examination of ground-based and space-based approaches to optical detection and tracking of artificial satellites.* United States.

[18] Clemens, S. (2019). *On-orbit resident space object (RSO) detection using commercial-grade star trackers*. York University, Toronto, Ontario.

[19] Swain, A. (2018, September 2). *Noise filtering in digital image processing*. Medium. https://medium.com/@anishaswain/noise-filtering-in-digital-image-processing-d12b5266847c

[20] Rush, Allen. (n.d.). *Comparing linear versus nonlinear filters in image processing*. Embedded Computing Design. https://embeddedcomputing.com/technology/analog-and-power/comparing-linear-versus-nonlinear-filters-in-image-processing#:~:text=Nonlinear%20filters%20have%20quite%20different,in%20a%20non%2Dintuitive%20manner.

[21] Veldhuizen, T. (1998, January 16). The Wiener Filter. https://homepages.inf.ed.ac.uk/rbf/CVonline/LOCAL_COPIES/VELDHUIZEN/node15.html#:~:text=The%20Wiener%20filter%20is%20the,in%20the%20random%20process%20sense

[22] 2-D adaptive noise-removal filtering - MATLAB. (n.d.). https://www.mathworks.com/help/images/ref/wiener2.html

[23] Jain, R. C., Kasturi, R., & Schunck, B. G. (1995). Chapter 5: Edge Detection. In *Machine vision*. essay, McGraw-Hill.

[24] Fisher, R., Perkins, S., Walker, A., & Wolfart, E. (2003). *Sobel Edge Detector*. https://homepages.inf.ed.ac.uk/rbf/HIPR2/sobel.htm

[25] Bernander, K. (2014). *A Method for Detecting Resident Space Objects and Orbit Determination Based on Star Trackers and Image Analysis*. Uppsala University, Sweden.

[26] Great Learning Team. (2022, December 13). *What is edge detection - an introduction*. Great Learning Blog https://www.mygreatlearning.com/blog/introduction-to-edge-detection/#:~:text=Edge%20detection%20is%20a%20technique,or%20boundaries)%20of%20the%20image

[27] Sahir, S. (2019, January 27). *Canny edge detection step by step in python - computer vision*. Medium. https://towardsdatascience.com/canny-edge-detection-step-by-step-in-python-computer-vision-b49c3a2d8123

[28] Axel, Wang, S., Pantelis, Clayton, Brickley, M., Richard, Aivar, Detken, K.-O., Yusuf, Javi, Aleix, Wen, S., & Ishan. (2018, April 28). *Asi183mm pro (mono)*. ZWO ASI. https://astronomy-imaging-camera.com/product/asi183mm-pro-mono/

[29] Peat, C. (n.d.). Heavens Above. https://www.heavens-above.com/

[30] Canadian Space Agency. (2018, July 25). *About Stratos, the CSA's Stratospheric Balloon Program*. https://www.asc-csa.gc.ca/eng/sciences/balloons/stratos.asp

[31] Kunalakantha, P., Vallecillo Baires, A., Dave, S., Clark, R., Chianelli, G., & Lee, R. S. (2023). Stratospheric night sky imaging payload for Space Situational Awareness (SSA). *Sensors*, *23*(14), 6595. https://doi.org/10.3390/s23146595

[32] Canadian Space Agency. (2023, July 5). *NEOSSat: Observing asteroids, space debris and exoplanets*. https://www.asc-csa.gc.ca/eng/satellites/neossat/

[33] Abbasi, V., Thorsteinson, S., Balam, D., Rowe, J., Laurin, D., Scott, L., & Doyon, M. (January, 2019). 1st NEO and Debris Detection Conference. In *THE NEOSSAT EXPERIENCE: 5 YEARS IN THE LIFE OF CANADA'S SPACE SURVEILLANCE TELESCOPE*. Darmstad, Germany.

[34] University of Calgary. (2016, December 23). *FAI*. e-POP. https://epop.phys.ucalgary.ca/fai/

[36] Cogger, L., Howarth, A., Yau, A. et al. Fast Auroral Imager (FAI) for the e-POP Mission. *Space Sci Rev* 189, 15–25 (2015). https://doi.org/10.1007/s11214-014-0107-x

[36] Clark, R., Fu, Y., Dave, S., & Lee, R. (2021). Simulation of RSO Images for Space Situation Awareness (SSA) Using Parallel Processing. *Sensors*, 21(23), 7868. https://doi.org/10.3390/s21237868

[37] Canadian Space Agency. (2012, June 1). *NEOSSat (near-earth object surveillance satellite)*. eoPortal. https://www.eoportal.org/satellite-missions/neossat#nessi-near-earth-space-surveillance-imager

[38] Zeiss, C. (n.d.) ZEISS *Dimension 2/25 Datasheet*. ZEISS. https://www.zeiss.com/content/dam/consumer-products/downloads/industrial-lenses/datasheets/en/dimension-lenses/datasheet-zeiss-dimension-225.pdf

[39] Jones, R. (2022). *On pixel size and image resolution*. Telescope Live. https://telescope.live/blog/pixel-size-and-image-resolution

[40] Burnett, G. (2018, June 26). *Rules (1-2 arc second per pixel) - and when the break them!*. Atik Cameras. https://www.atik-cameras.com/news/rules-1-2-arc-second-per-pixel-and-when-to-break-them/

[41] The SciPy Community. (2008-2023). *Scipy.signal.wiener*. SciPy v1.11.4 Manual. https://docs.scipy.org/doc/scipy/reference/generated/scipy.signal.wiener.html

[42] Fowler, M. (n.d.). *Wiener Filter for Deterministic Blur Model* [Slides]. EE522 estimation theory. http://ws.binghamton.edu/fowler/fowler%20personal%20page/EE522.htm

[43] The Scikit-Image Team. (2013-2023). *Skimage.morphology*. Skimage 0.22.0 Documentation. https://scikit-image.org/docs/stable/api/skimage.morphology.html#skimage.morphology.remove_small_holes

[44] Zhu, W., Zeng, N., & Wang, N. (2010). Sensitivity, Specificity, Accuracy, Associated Confidence Interval and ROC Analysis with Practical SAS® Implementations. K&L Consulting Services, Inc., Octagon Research Solutions.

[45] Armellin, R., Di Lizia, P., & Zanetti, R. (201+-+6). Dealing with uncertainties in angles-only initial orbit determination. *Celestial Mechanics and Dynamical Astronomy, 125*(4), 435–450. https://doi.org/10.1007/s10569-016-9694-z

[46] Pastor, A., Sanjurjo-Rivo, M., & Escobar, D. (2021). Initial orbit determination methods for track-to-track association. *Advances in Space Research, 68*(7), 2677–2694. https://doi.org/10.1016/j.asr.2021.06.042

[47] Porras-Hermoso, A. (n.d). Orbit determination of RSOs in LEO orbits, using only optical data.

[48] Rhodes, B. (2023). *sgp4 2.23*. PyPI. https://pypi.org/project/sgp4/

[49] Curtis, H. D. (2014). *Orbital Mechanics for Engineering Students*. Elsevier Butterworth-Heinemann.

[50] Li, C. (2023). *Welcome to the ORBDTOOLS package*. GitHub. https://github.com/lcx366/ORBDTOOLS/blob/main/